Metapopulations in miniature:
connectivity, subpopulation extinction, and recovery in microbial microcosms

By

Helen Kurkjian

A dissertation submitted in partial satisfaction of the

requirements for the degree of

Doctor of Philosophy

in

Integrative Biology

in the

Graduate Division

of the

University of California, Berkeley

Committee in charge:

Professor Ellen Simms, Chair
Professor David Ackerly
Professor Steven Lindow
Professor Laurel Larsen

Spring 2018

Abstract

Metapopulations in miniature: connectivity, subpopulation extinction, and recovery in microbial microcosms

by

Helen Kurkjian

Doctor of Philosophy in Integrative Biology
University of California, Berkeley

Professor Ellen Simms, Chair

Metapopulations occupy spatially divided habitats and understanding how that fragmentation affects their survival, growth, dispersal, and persistence is critical to their conservation. Researchers in many sub-fields of ecology and evolutionary biology test hypotheses relating to metapopulation dynamics and landscape spatial structure. Key aspects of these hypotheses are sometimes (a) large numbers of subpopulations and dispersal corridors and (b) their positions relative to each other. Comparing such spatial hypotheses using traditional lab equipment and methods is impractical, unwieldy, expensive, or impossible.

I invented the Metapopulation Microcosm Plate (MMP) to overcome these drawbacks. This device resembles a 96-well microtiter plate; the 96 wells represent habitat patches and they are connected by dispersal corridors that can be modified in their spatial position to create various artificial landscapes, with hundreds of non-intersecting dispersal corridors of varying lengths. The device can be filled with nutrient broth and used to culture microbial metapopulations.

In Chapter One, I first demonstrate that bacterial travel time is significantly faster through MMP dispersal corridors that are shorter, but is unaffected by corridor vertical position within the plate. Thus, MMPs satisfy the necessary assumptions for use in metapopulation experiments. Furthermore, travel time by bacteria with fully functional flagella was significantly faster than that of bacteria with disabled flagella, indicating that the bacteria actively swim through the corridors, rather than traveling by simple diffusion. Thus, MMPs can test hypotheses that account for behavioral responses. MMPs can be used to test many spatial hypotheses that have previously been prohibitively difficult to test. Further, by incorporating individual behavioral responses to within-patch conditions, MMPs incorporate greater realism than do directed pipetting or other artificial dispersal methods.

In Chapter Two, I used MMPs to explore how recolonization and recovery after subpopulation extinction differs in metapopulations in which the dispersal corridors have different spatial arrangements. Some metapopulations have corridors spread relatively evenly through space in a homogeneous arrangement such that most subpopulations are connected to a few neighbors, while others have corridors clustered in a heterogeneous arrangement, creating a

few highly connected subpopulations and leaving most subpopulations with only one or two neighbors. Graph theory and empirical data from other biological and non-biological networks suggest that heterogeneous metapopulations should be the most robust to subpopulation extinction. Here, I compared the recovery of metapopulations with homogeneous and heterogeneous corridor arrangements following small, medium, and large subpopulation extinction events. I found that while metapopulations with heterogeneous corridor arrangements had the fastest rates of recovery following extinction events of all sizes and had the shortest absolute time to recovery following medium-sized extinction events, metapopulations with homogeneous corridor arrangements had the shortest time to recovery following the smallest extinction events.

Finally, for Chapter Three I conducted an experiment to test whether metapopulations with heterogeneous corridor arrangements recover more slowly from extinctions targeted at high connectivity subpopulations than random extinctions in low connectivity subpopulations. Simulations of the World Wide Web and other heterogeneous networks have demonstrated that, while they are very robust to random loss of nodes, targeted attacks on highly connected nodes can lead to failure of the entire network. Based on these simulations, I predicted that metapopulations with heterogeneous corridors would recover fastest when extinctions occurred in low connectivity wells, regardless of extinction event size. Unlike in theoretical networks, however, the corridor arrangements of metapopulations cultured in MMPs cannot be completely homogeneous, because wells on the edge will be slightly less connected than those in the center. However, I predicted that a small deviation in connectivity would be unimportant and that recovery in metapopulations with homogeneous corridors would not be affected by whether extinctions were in low connectivity or high connectivity wells. Instead, I found that, at both low and medium levels of extinction targeted at highly connected subpopulations, both heterogeneous and homogeneous metapopulations recovered more quickly when those extinctions were targeted at high connectivity wells, but that when many subpopulations went extinct, all metapopulations recovered fastest when those extinctions were in low connectivity wells.

This work demonstrates that MMPs can be used to test the assumptions of metapopulation theory, especially those involving large numbers of subpopulations and dispersal corridors. I have shown that metapopulations with heterogeneous corridor arrangements have the fastest rates of recovery from subpopulation extinction, but that that faster rate only translates to a shorter absolute time of recovery after larger extinction events. Furthermore, when smaller numbers of subpopulations go extinct, metapopulations recover more quickly when those extinctions are targeted at high connectivity subpopulations, but when large numbers of subpopulations go extinct, recovery is faster when low connectivity subpopulations are targeted. This suggests that dispersal corridors that are clustered in space may help to alleviate the effects of habitat fragmentation in some circumstances, but exacerbate them in others.

For my parents,
Diane and Mark Kurkjian,
whose encouragement helped me to begin this work.

And for
Nick Jourjine,
whose support helped me to finish it.

TABLE OF CONTENTS

LIST OF TABLES

LIST OF FIGURES

ACKNOWLEDGEMENTS

I wish to express my deep gratitude to Dr. Ellen Simms for her guidance in all stages of this project. She let me fail until I succeeded, which was a valuable experience for which I am profoundly thankful. Not every advisor would have continued to encourage this project after the first few melted, leaking plates, but I am very grateful that she did. She allowed me to pursue a project that was a little bizarre and helped me to make it the best work I could.

I would also like to thank the many current and former Simms Lab members who gave me friendship and support, as well as valuable comments and suggestions on the scope of this project, design of experiments, and manuscript drafts. Thanks to Dr. Kimberly La Pierre, Dr. Stephanie Porter, Dr. Samuel Diaz-Munoz, Rebecca Welch, Briana Boaz, Dr. Marriam Zafar, Dr. Mohsin Tariq, and Georgia Gregory. And many thanks to Monica Sadhu and Teffany Bareng for their assistance in the lab when this project was in its earliest and most frustrating stages.

My dissertation committee, Dr. David Ackerly, Dr. Laurel Larsen, and Dr. Steven Lindow provided many helpful discussions and constructive suggestions. I am deeply grateful for their support, for their advice on my project proposal and experiments, and for their many comments on this dissertation. I would also like to thank the Lindow Lab, especially Monica Hernandez and Tyler Helmann, for generously providing me with bacterial cultures and microbiological advice. And I would like to thank Dr. Caroline Williams and the Williams Lab for kindly allowing me to use their lab equipment for my data collection. I would also like to thank Dr. Luis Gillarranz for helpful conversations and comments on my experiments.

Early conversations with Dr. Thomas Libby and Dr. Shawn Shirazi were instrumental in developing the first concept of this project. Without their introduction to the tools and materials I used, I never would have had the confidence to begin. I am genuinely obliged to them for this support. I also wish to acknowledge the assistance provided by the staff of the Jacobs Institute for Design Innovation. And I am grateful to the Center for Integrative Biomechanics in Education and Research for allowing me to use their equipment. I am also very grateful to Aaron Pomerantz for photography assistance.

I wish to thank Dr. Erik Jules and April Sahara for supporting me during my master's and inspiring me to pursue a doctorate.

I would like to express my very great appreciation to my family, especially my parents Diane and Mark Kurkjian and my brother Gregory Kurkjian for encouraging me to continue my education for the past three decades. I would not be here without their support.

Finally, I would particularly like to thank Dr. Nicholas Jourjine, who made me dinner while I was working, helped me collect data in the middle of the night, and without whose support I would have had much less fun while completing this project.

This work was supported financially by a National Science Foundation Doctoral Dissertation Improvement Grant [DEB-1601762], grants from Sigma Xi National and UC Berkeley Chapter, the Roy Leeper Scholarship for the Biological Sciences, and the Reshetko Family Scholarship of the College of Letters and Sciences.

CHAPTER 1

The Metapopulation Microcosm Plate:
A modified 96-well plate for use in microbial metapopulation experiments

Introduction

Many populations occupy spatially fragmented habitats and, while landscapes can be naturally patchy, excessive human-caused habitat fragmentation is a leading threat to biodiversity (Millenium Ecosystem Assessment, 2005; Hanski, 2011). Artificial dispersal corridors within or between habitat fragments, especially when those fragments are biological preserves, are an important strategy to compensate for this fragmentation (Rosenberg & Noon, 1997; Chetkiewicz, St. Clair, & Boyce, 2006). To create a corridor network that can promote dispersal we must understand how their characteristics contribute to the survival, growth, and dispersal of populations.

When populations in fragmented habitats are idealized as a network of subpopulations in patches of suitable habitat, connected by dispersal, and surrounded by a matrix of less suitable habitat, they are commonly referred to as metapopulations (Hanski, 1991). Using the metapopulation framework to predict growth, dispersal, and higher-order metapopulation dynamics involves assumptions about subpopulations and dispersal corridors (Amarasekare, 1998; Parker, 1999; Hanski & Ovaskainen, 2000). Thus, to guide conservation efforts with metapopulation models we must test their assumptions and predictions experimentally to determine which are best supported by data (Kareiva, 1989; Holyoak & Lawler, 2005). The degree to which dispersal corridors increase survival and growth of populations of conservation interest can depend on their length, width, shape, position on the landscape, and habitat quality, among other characteristics. Thus, understanding how dispersal corridors alleviate the impacts of fragmentation requires theoretical and experimental models that include these factors.

Starting with Huffaker's famous 1958 experiment demonstrating the role of spatial heterogeneity in predator-prey oscillations (Huffaker, 1958), many experimental tools have been developed to examine how different spatial characteristics affect the dynamics of metapopulations (*e.g.* Cadotte, 2007; Fellous, Duncan, Coulon, & Kaltz, 2012; Keymer, Galajda, Muldoon, Park, & Austin, 2006; Warren, 1996). These tools have highlighted how landscape structure mediates population processes, leading to ever-more complex spatial hypotheses. For example, Gilarranz and Bascompte (2012) used computer simulations of a variation of the Levins (1969) model to predict how different spatial arrangements of dispersal corridors affected persistence of metapopulations. In the simulations, topologies ranged from entirely homogeneous networks, in which every subpopulation was connected to the same number of neighbors, to strongly heterogeneous spatial configurations, in which the number of neighbors per subpopulation followed a power-law distribution. Such a complex hypothesis must be tested using tools that can produce larger and more complex replicable experimental metapopulations. For example, approximating a power-law distribution of neighbor-connections in an experimental set up requires a minimum of dozens of subpopulations and dispersal corridors.

Several experimental systems have been developed to cope with the physical constraints of creating a replicable metapopulation of this size, including arrays of jars or flasks connected by tubing (e.g. Fjerdingstad, Schtickzelle, Manhes, Gutierrez, & Clobert, 2007), controlled dispersal among containers via hand or robotic pipetting (e.g. Fox, Vasseur, Cotroneo, Guan, & Simon, 2017), or passive dispersal through channels in microfluidics devices (e. g. Keymer et al., 2006). These systems are valuable, but feature important limitations. For example, a system of jars and tubes is sufficient to examine dispersal between two or a few subpopulations, but quickly becomes unwieldy for dozens or more. Hand or robotic pipetting mimics passive dispersal, but fails to account for the possibility that dispersing individuals may not be a random subset of the population (Altermatt et al., 2015). And while microfluidics technology can allow for behavioral responses to patch conditions and has greatly expanded its 3D capabilities in recent years (Hol & Dekker, 2014; Chiu et al., 2017), such methods can be costly and require technology that may be inaccessible to many researchers. I therefore invented the Metapopulation Microcosm Plate (MMP), a device that resembles a 96-well microtiter plate, but contains corridors that connect the wells (Figure 1.1). MMPs can be filled with nutrient broth and used to culture microbial metapopulations or metacommunities. Here, I demonstrate that MMPs meet the necessary requirements and physical parameters to effectively test hypotheses about the spatial configuration of dispersal corridors in complex metapopulations.

Methods

Construction and Set-up

Metapopulation Microcosm Plates are assembled on the benchtop from layers of plastic and rubber which can themselves be designed, modified, and fabricated using technology now commonly found in many research facilities, university campuses, public schools, and community-based makerspaces (Lou & Peek, 2016). The top and bottom layers are made from 4.750 mm and 3.175 mm thick polycarbonate, respectively, and sandwich the interior layers of five 0.51 mm thick silicone rubber gaskets alternating with four 0.76 mm polycarbonate sheets (Figure 1.1). Corridors are cut to a depth of 0.51 mm in the 0.76 mm interior polycarbonate layers. All layers can be washed and reused, but the interior corridor layers are changed between experiments to create different spatial configuration treatments. I designed all component pieces in Autodesk Fusion 360 (Autodesk, Inc., San Rafael, CA, USA), cut all polycarbonate pieces on a CNC-controlled desktop milling machine (Othermill Pro; Bantam Tools, Berkeley, CA, USA), and cut the silicone gaskets on a laser cutter (Universal Laser Systems, Inc., Scottsdale, AZ, USA).

Each MMP is assembled using 35 2-56 x 19.05 mm stainless steel screws and hex nuts (Figure 1.2a), which are first loosely tightened by hand (Figure 1.2b). The loosely assembled MMP is placed in a small Pyrex dish, covered in aluminum foil, sterilized in an autoclave on a 30 min dry cycle at 121°C (Figure 1.2c), and allowed to cool before the screws are tightened to 0.339 newton-meters (Figure 1.2d). Postponing final tightening until after autoclaving prevents warping of the polycarbonate pieces. The fully assembled MMP remains in its sterile Pyrex dish, which is then filled with sterile nutrient broth (Figure 1.2e). In a process similar to that used for filling microfluidics devices (Monahan, Gewirth, & Nuzzo, 2001), the broth-filled dish is placed in a vacuum chamber for three 30-minute intervals, each separated by at least 30-

minutes, and agitated gently twice per vacuum interval (Figure 1.2f). This treatment fills all corridors and wells with nutrient broth. The MMP is removed from the broth (Figure 1.2g), excess broth is suctioned from its surface, which is subsequently rinsed with sterile water followed by 70% ethanol (Figure 1.2h). Since each well has been filled to its maximum volume of 150 µL, 10 µL must be removed from each well to bring it down to its maximum working volume of 140 µL. The MMPs can now be inoculated and used to culture a microbial metapopulation or metacommunity. Because the exterior dimensions match a standard 96-well microtiter plate, the size of each subpopulation can be tracked over time on a spectrophotometric plate reader.

In all experiments described here, MMPs were filled with Luria-Bertani liquid medium (LB; Cold Spring Harbor Protocols, 2006) containing 40 µg/mL nitrofurantoin. MMPs used to culture flagellar mutant strains also contained 15 µg/mL tetracycline to select against loss of mutant plasmids. Corridor length and vertical position experiments were performed using wild type *Pseudomonas syringae* pv. *syringae* B728a, which doubles approximately every 3 h at 15°C in this set-up. The flagellar mutant used in the corridor length experiment was *Pseudomonas syringae* pv. *syringae* B728a Δ*flgK*. All *Pseudomonas* strains were provided by the Lindow Lab, UC Berkeley. All analyses were performed in R (R Core Team, 2016).

Evaporation, Edge Effects, and Sterility

To test the hypotheses that total evaporation, evaporation edge effects, and ability to maintain sterility of an MMP is comparable to that of a commercially available standard round-bottom 96-well microtiter plate (Thermo Fisher Scientific, Waltham, MA, USA), I constructed and filled 12 MMPs with no corridors in their interior layers using the methods described above.

I used a micropipettor to fill each well of 12 control microtiter plates with 200 uL of broth. In each MMP and microtiter plate I mimicked a standard liquid needle inoculation using sterile nutrient broth. The perimeter of each plate and MMP was sealed with Parafilm® M Sealing Film (Beamis NA, Neenah, WI, USA) and all were incubated at 15°C. After 1, 3, 5, and 7 days, three MMPs and three control microplates were opened and the contents of every well was stab cultured to test sterility and then extracted and weighed to measure evaporation.

To compare total evaporation among plates, I calculated the coefficient of variation of well weight for each MMP and microplate and performed a two-way ANOVA with plate type (MMP or microplate) and days after filling (1, 3, 5, or 7) as explanatory variables. To examine evaporative edge effects, I calculated the mean deviation of the weight of inner wells and edge wells for each MMP and microplate, standardized to plate mean, as the response variable and performed a two-way ANOVA with plate type and days after filling as explanatory variables. Levene's and Anderson-Darling tests demonstrated that the assumptions of homogeneity of variance and normality, respectively, were met for both response variables.

Corridor Vertical Position

Corridors in the four interior layers of an MMP can intersect a well at any of four vertical levels. To test the hypothesis that bacteria can enter the corridors of any level equally well, I conducted an experiment to compare bacterial travel time through corridors of equal length in each of the four possible levels. A treatment in this experiment consisted of one MMP with 48 pairs of wells, each pair connected by a single 4.0 mm long corridor, with all corridors in a single

interior layer. In each of the four treatments, the corridor layer was placed in a different vertical position. Each MMP was filled as described above and one well of each connected pair was inoculated from a liquid culture. Optical density (OD) at 600 nm was measured every 10 minutes for 72 hours. I calculated time-to-detectability, the time it took each well to reach a detectable concentration of bacteria, where detectable OD was defined as 120% of a well's OD immediately following inoculation. I calculated travel time by subtracting time to detectability of the inoculated well from the time to detectability of its connected uninoculated well. To compare travel time through corridors in the four different interior layers, I conducted a one-way ANOVA using travel time as the response variable and interior layer (1, top – 4, bottom) as the explanatory variable. Levene's and Anderson-Darling tests demonstrated that the assumptions of homogeneity of variance and normality were met for this ANOVA.

Corridor Length and Travel Time of Bacteria with and without Functional Flagella

To test the hypothesis that bacteria can actively move through corridors and are not simply diffusing, I compared the travel time of wild-type *P. syringae* pv. *syringae* B728a, which have functional flagella, to that of *P. syringae* pv. *syringae* B728a Δ*flgK*, in which the flagella are inactivated. In this experiment, every MMP contained a single corridor layer with six corridors of each of the following lengths: 4.0 mm, 7.823 mm, 15.113 mm, 24.536 mm, and 34.417 mm. Each corridor connected one pair of wells, one well of which was inoculated with either *Pseudomonas syringae* pv. *syringae* B728a or *P. syringae* pv. *syringae* B728a Δ*flgK*. Optical density (OD) at 600 nm was measured every 10 minutes for 72 hours. Travel time was calculated as described above. To compare travel time by the two strains through corridors of different lengths, I conducted an ANCOVA using travel time as the response variable, strain (wild-type or flagellar mutant) as the categorical variable, and corridor length as the continuous explanatory variable. Levene's and Anderson-Darling tests demonstrated that the assumptions of homogeneity of variance and normality were met for this ANCOVA.

Results

Evaporation, Edge Effects, and Sterility

A two-way ANOVA (Table 1.1) of the total evaporation at 15°C response variable showed no significant main effect of plate type, nor an interaction of days and plate type, but there was a significant main effect of days after filling (Figure 1.3A; $F_{3,16} = 16.897$, $p < 0.001$). Post-hoc analysis using Tukey's Honestly Significant Difference (HSD) showed no significant differences among 1, 3, and 5 days after filling, whereas 7 days after filling differed from the other 3 treatments (day 1-7, $p_{HSD} < 0.001$; day 3-7, $p_{HSD} < 0.001$; day 5-7, $p_{HSD} < 0.001$).

A two-way ANOVA (Table 1.2) of the edge effects response variable showed significant main effects of plate type (Figure 1.3B; $F_{1,16} = 51.303$, $p < 0.001$) and days after filling ($F_{3,16} = 4.174$, $p = 0.023$), with days 1 and 7 differing significantly from each other ($p_{HSD} = 0.017$). There was also a significant interaction between plate type and day ($F_{3,16} = 5.221$, $p = 0.011$), with significant interactions between plate type and days 1 and 5 ($p_{HSD} = 0.002$), days 1 and 7 ($p_{HSD} < 0.001$), days 3 and 7 ($p_{HSD} = 0.013$), and days 5 and 7 ($p_{HSD} = 0.006$).

Stab cultures of all wells from all plates were sterile.

Corridor Vertical Position

A one-way ANOVA (Table 1.3) of travel time between wells with vertical position of dispersal corridor as the explanatory variable was not significant (Figure 1.4; $F_{3,170} = 0.688$, $p = 0.560$), demonstrating that bacteria were able to enter corridors in all four interior layer vertical positions equally well.

Distance Travelled by Bacteria with and without Functional Flagella

The ANCOVA (Table 1.4) found a significant positive relationship between corridor length and travel time (Figure 1.5; $F_{1,64} = 71.383$, $p < 0.001$), a significant main effect of strain on travel time ($F_{1,64} = 116.131$, $p < 0.001$), and a significant interaction ($F_{1,64} = 31.658$, $p < 0.001$), in which the flagellar mutant had a steeper relationship between corridor length and travel time.

Discussion

A great strength of ecology and evolutionary biology is that these fields use many experimental, mathematical, and statistical models to manipulate and reduce biological complexity. Experimental microcosms are physical models that constitute a key component of this toolkit. The utility of microcosms in ecology and evolutionary biology is hotly debated (Carpenter, 1996; Srivastava et al., 2004), because of their extreme position in the apparent tradeoff between realism and experimental tractability. Despite the challenges involved in generalizing their results, microcosms have provided many key ecological insights, including a more detailed understanding of chemical cycling in soil, water, and air, the impacts of heavy metals, and the effects of environmental changes on food web structure, among many others (Beyers & Odum, 1993; Fraser & Keddy, 1997; Altermatt et al., 2015).

In the struggle to understand the natural world, microcosms make tractable the elements that most resist manipulation in nature and it is difficult to identify an element more resistant to experimental manipulation than complex landscape spatial structure. For example, cougars may disperse as far as 2450 km (Hawley et al., 2016) through urban and rural habitats, over mountains, across rivers, and through cities. A manipulative experiment to test the effects of dispersal corridor placement on cougar population dynamics would require continental-scale experimental replicates, which are financially and practically infeasible. And yet, understanding such relationships is critical to conservation planning (Morrison & Boyce, 2009). To bridge this knowledge gap, where species of conservation concern often grow, develop, and move on intractably large spatial and temporal scales, we must develop tools that allow us to reduce the complexity of landscape spatial structure, break it into simpler, more manageable parts, and manipulate it to explore causality.

In their 2002 review of experimental approaches to spatial fragmentation, McGarigal and Cushman describe their ideal manipulative field experiment. This experiment would use replicate experimental landscapes of a biologically relevant size, but which could be manipulated in their spatial extent and configuration of fragmentation. It would include adequate temporal and spatial controls and be observed on a time scale long enough to account for potential time

lags (McGarigal & Cushman, 2002). Although excellent field experiments exist which meet many of the proposed criteria, the intervening years have not seen a complete achievement of these goals for any macroscopic organism. Landscape microcosms for microorganisms offer an opportunity to meet all these requirements.

Microorganisms have long served as model organisms in ecology. In their review of microbial model systems in ecology, Jessup *et al*. (2004) cite W.H. Dallinger's (1887) experimental evolution studies, which he described in his presidential address to the Royal Microscopy Society in 1887, as the first published record of a microbial microcosm experiment. Since that time, key ecological insights obtained from microbial experiments include Woodruff's (1911) measurements of density-dependent growth in single-species cultures of *Paramecium spp.*, Gause's (1934) demonstrations of competitive exclusion in mixed assemblages of those same species, and Hairston *et al*.'s (1968) experiments exploring the diversity-stability relationship using *Paramecium spp*. in multitrophic communities with bacteria and protozoans. From the mid-20th century onward, microbial model systems have exploded in popularity and examples of their use can be found in virtually every subfield of ecology (reviewed in Jessup, Forde, & Bohannan, 2005).

Microbial microcosm studies of metapopulation (Keymer et al., 2006; Fox et al., 2017; Gilarranz, Rayfield, Liñán-Cembrano, Bascompte, & Gonzalez, 2017) and metacommunity (Guelzow, Muijsers, Ptacnik, & Hillebrand, 2017; Resetarits, Cathey, & Leibold, 2018) dynamics are also increasingly common, although some authors dismiss the effects of spatial structure on microbial population dynamics as fundamentally different from those on macroscopic organisms (Carpenter, 1996). But just as prokaryotic and eukaryotic microbial organisms share an abundance of genetic, reproductive, and metabolic similarities with macroscopic organisms, they likewise share many movement-related characteristics (Jessup et al., 2005). They can move at random or make directed moves towards or away from chemical and/or physical stimuli, as well as respond behaviorally to the presence of con-specifics, resources, or predators. And while it is sometimes argued that microcosms operate on time and spatial scales that are too short to be generalizable, a major virtue is that they can run for longer durations and at larger spatial scales relative to microbial lifespans and cell sizes (Ives, Foufopoulos, Klopfer, Klug, & Palmer, 1996; Jessup et al., 2005).

Theoretical metapopulation models have explored a variety of possible spatial relationships between the elements traditionally included in metapopulations: patches, dispersal pathways, and the background matrix. For a physical model to be a useful analogue to any of those theoretical formulations, it must allow researchers to manipulate interesting elements. Like all methods for reproducing spatial structure, the Metapopulation Microcosm Plate allows us to manipulate some elements but not others, which suits it for testing a particular subset of spatial hypotheses. In this paper, I have demonstrated that the MMP is a valid (Rykiel, 1996) physical experimental model for comparing the effects of corridor size and position on microbial metapopulations or metacommunities. All wells can persist as uniform habitat patches, organisms are equally able to enter any dispersal corridor, and their travel through dispersal corridors is affected by corridor length but not corridor level. By demonstrating that MMP sterility and evaporative edge effects remain comparable to those of other standard lab equipment over a reasonable time duration, I established that wells can be maintained as uniform habitat patches. Showing that travel time to adjacent wells is the same through corridors at any vertical position confirms that organisms are equally able to enter any dispersal corridor. Finally, by showing that bacteria take more time to travel through longer dispersal corridors and

that actively motile bacteria move faster than those limited to movement via diffusion, I have demonstrated that travel across these artificial landscapes is in those respects similar to movement of other types of organisms across landscapes.

As models with which to manipulate corridor length and width, patch size and shape, and corridor position within metapopulations, MMPs can test hypotheses about how spatial structure and connectivity affect metapopulation and metacommunity dynamics, including metapopulation persistence, species diversity, community stability, predator-prey dynamics, competition, facilitation, and the evolution of dispersal. As described earlier, Gilarranz and Bascompte (2012) hypothesized a relationship between the architecture of spatial networks and metapopulation persistence. To ask whether real organisms in metapopulations exhibit such a relationship would require an experimental system with multiple, replicable metapopulations, each with dozens or hundreds of subpopulations and corridors. The MMP provides a compact, inexpensive, tractable physical model for answering this question.

In summary, MMPs allow for many subpopulations and dispersal corridors, can be monitored using tools available for a standard 96-well microtiter plate (*e.g.* spectrophotometric plate reader), and are within the technical and financial means of many ecologists. Any organism cultured in an MMP must be able to live and move in liquid medium and be small enough to pass through the corridors. The corridors themselves, however, are easily modified in their width, curvature, and position relative to the wells or to other corridors. In its present configuration, the MMP is constrained by having a maximum of 96 equally-sized and -shaped wells in a fixed 8 x 12 rectangular array. However, patch size could be modified (within the constraints of the plate reader format), the number of interior layers could be increased to allow for more corridors, and corridor size (absolute or relative to organism size) could be manipulated by adjusting corridor depth or width. Further, more patches could be added by scaling up to the standard 384-well plate format. The Metapopulation Microcosm Plate is a flexible, affordable tool with which to explore metapopulation dynamics.

Table 1.1. A) Analysis of variance table for two-way ANOVA of the total evaporation at 15℃ response variable. Explanatory variables are plate type (MMP or microplate) and days after filling (1, 3, 5, or 7). B) Tukey's Honestly Significant Difference adjusted p-values for pairwise comparisons of days after filling.

A)

	df	SS	MS	*F*	*p*
Type	1	1.408E-04	1.408E-04	2.762	0.116
Days	3	2.584E-03	8.613E-04	16.897	**<0.001**
Type x Days	3	9.563E-05	3.188E-05	0.6254	0.609
Residuals	16	8.155E-04	5.097E-05		

B)

Days	p_{HSD}
1-3	0.412
1-5	0.140
1-7	**<0.001**
3-5	0.892
3-7	**<0.001**
5-7	**<0.01**

Table 1.2. A) Analysis of variance table for two-way ANOVA of the evaporative edge effects response variable. Explanatory variables are plate type (MMP or microplate) and days after filling (1, 3, 5, or 7). B) Tukey's Honestly Significant Difference adjusted p-values for pairwise comparisons of days after filling. C) Tukey's Honestly Significant Difference adjusted p-values for pairwise comparisons of interaction between plate type and days after filling.

A)	*df*	SS	MS	*F*	*p*
Type	1	1.355E-04	1.355E-04	51.303	**<0.001**
Days	3	3.307E-05	1.102E-05	4.174	**0.023**
Type x Days	3	4.136E-05	1.379E-05	5.221	**0.011**
Residuals	16	4.225E-05	2.641E-06		

B) Days	p_{HSD}
1-3	0.106
1-5	0.116
1-7	**0.017**
3-5	0.995
3-7	0.774
5-7	0.634

C) Type x Days	p_{HSD}
MMP:1-control:1	0.201
control:3-control:1	0.213
MMP:3-control:1	**0.046**
control:5-control:1	0.999
MMP:5-control:1	**0.002**
control:7-control:1	0.995
MMP:7-control:1	**<0.001**
control:3-MMP:1	>0.999
MMP:3-MMP:1	0.988
control:5-MMP:1	0.445
MMP:5-MMP:1	0.233
control:7-MMP:1	0.533
MMP:7-MMP:1	**0.014**
MMP:3-control:3	0.984
control:5-control:3	0.464
MMP:5-control:3	0.221
control:7-control:3	0.553
MMP:7-control:3	**0.013**
control:5-MMP:3	0.125
MMP:5-MMP:3	0.666
control:7-MMP:3	0.162
MMP:7-MMP:3	**0.070**
MMP:5-control:5	**0.005**
control:7-control:5	>0.999
MMP:7-control:5	**<0.001**
control:7-MMP:5	**0.006**
MMP:7-MMP:5	0.773
MMP:7-control:7	**<0.001**

Table 1.3. Analysis of variance table for one-way ANOVA of travel time between wells with vertical position of dispersal corridor as the explanatory variable.

	df	SS	MS	*F*	*p*
Vertical Position	3	34101	11367	0.688	0.560
Residuals	170	2807715	16516		

Table 1.4. Analysis of variance table for ANCOVA of travel time between wells with corridor length as continuous explanatory variable and strain (with or without functional flagella) as categorical explanatory variable.

	df	SS	MS	*F*	*p*
Length	1	2758881	2758881	114.980	**<0.001**
Strain	1	3882758	3882758	161.818	**<0.001**
Length x Strain	1	1021001	1021001	42.551	**<0.001**
Residuals	64	1535651	23995		

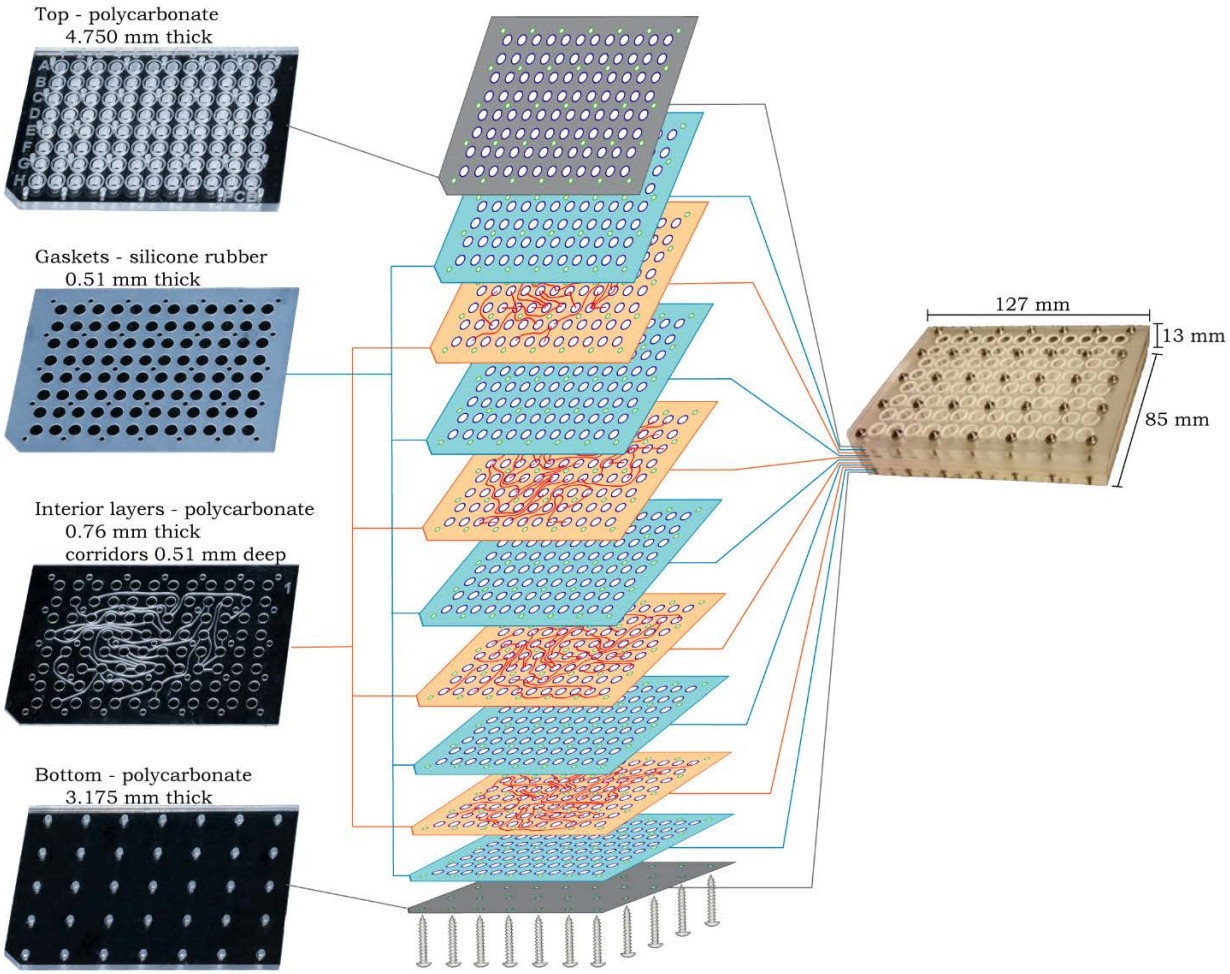

Figure 1.1. Metapopulation Microcosm Plate. Left) Photographs (oblique view) of top, gasket, interior layer, and bottom. Center) Exploded diagram, with top and bottom in gray, gaskets in light blue, interior layers in peach, 96 wells outlined in dark blue, 35 screw holes outlined in green, and 176 corridors indicated by red lines. Right) Photograph (oblique view) of assembled MMP. Photo credit (Aaron Pomerantz)

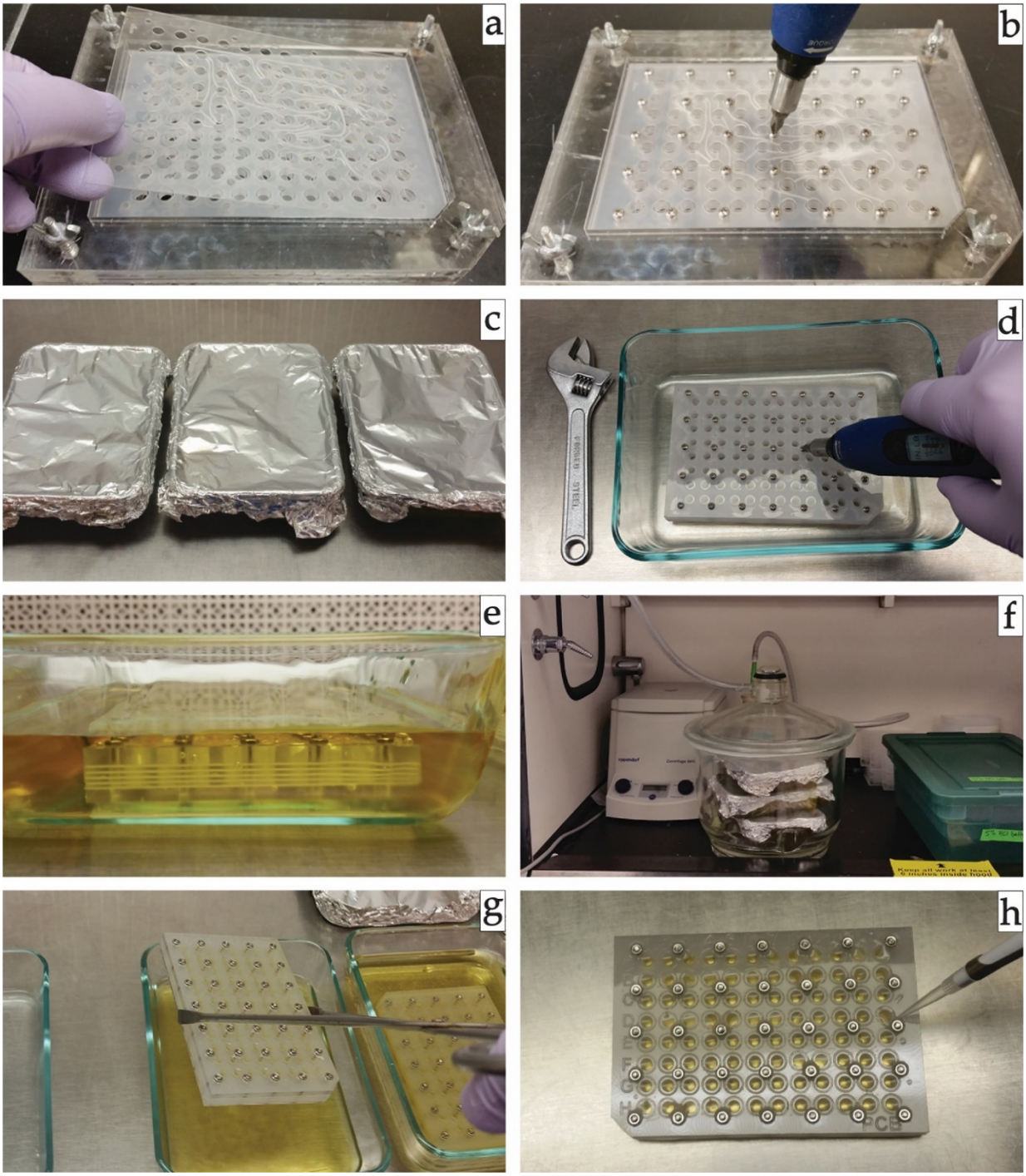

Figure 1.2. Metapopulation Microcosm Plate assembly and filling. a) stack and align layers b) tighten screws finger-tight c) autoclave d) tighten screws to 0.339 newton-meters e) cover with nutrient broth f) place in vacuum chamber g) remove from broth h) clean exterior.

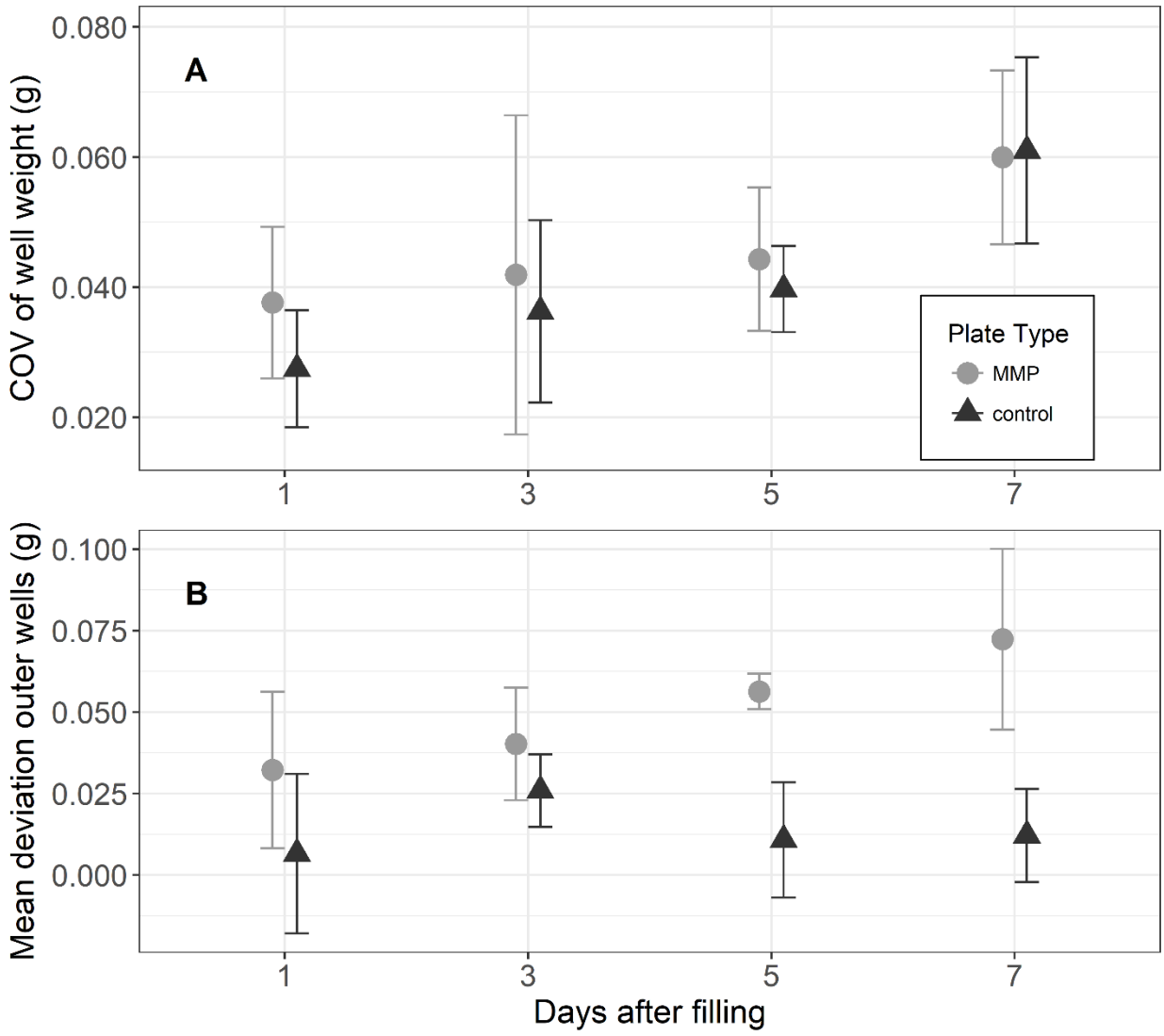

Figure 1.3. A) Overall evaporation did not differ between MMPs and microplates, but was significantly higher after 7 days for all plates. B) Edge effects (weight differences between the remaining contents of interior and exterior wells) were equal in magnitude for MMPs and microplates after 1 and 3 days, but larger in MMPs after 5 and 7 days.

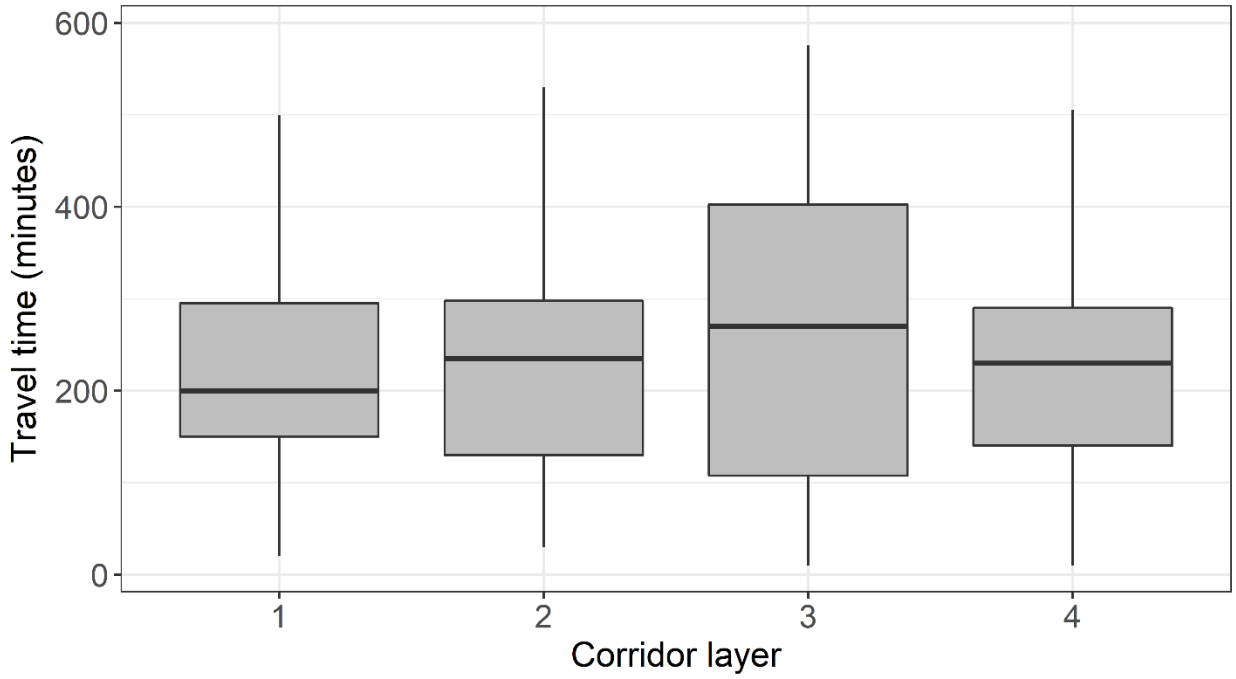

Figure 1.4. Bacteria could enter corridors in all four interior layers equally well.

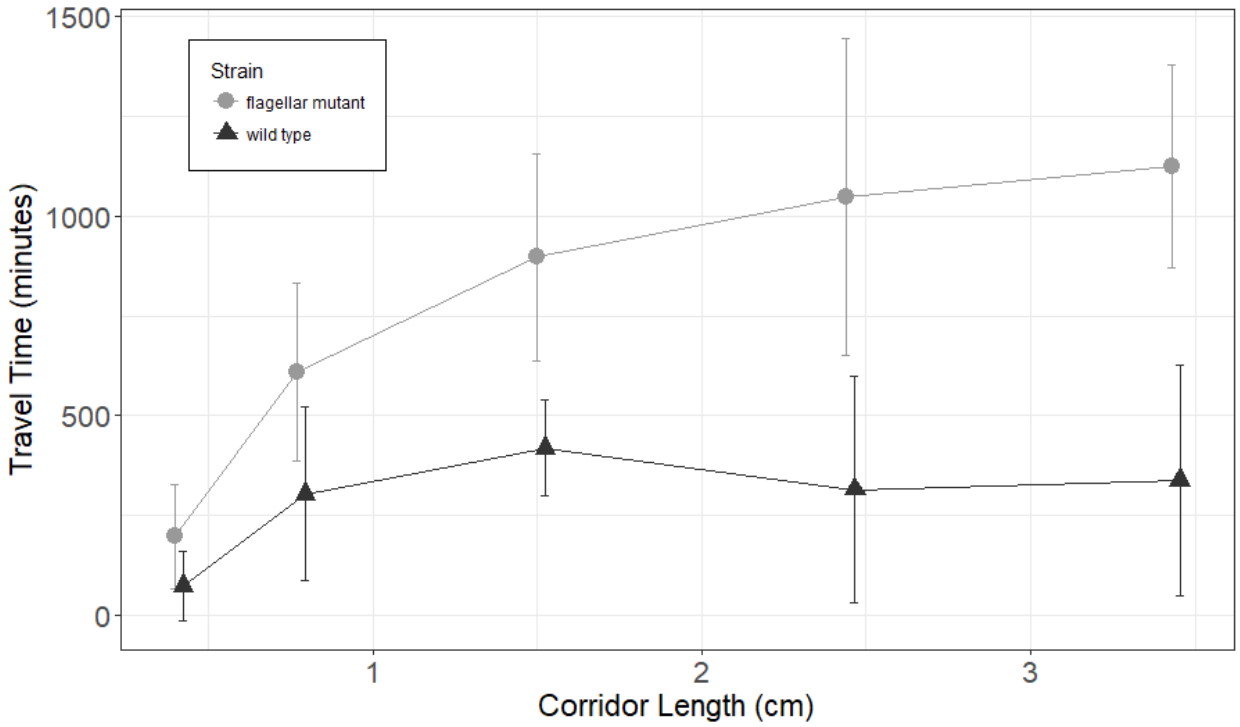

Figure 1.5. Bacteria take more time to travel down longer corridors. Mutants lacking a functional flagellum take more time to travel down corridors via diffusion than wild type bacteria with a functional flagellum.

CHAPTER 2

Clustering of dispersal corridors in metapopulations leads to higher rates of recovery following subpopulation extinction

Introduction

A metapopulation is a collection of subpopulations occupying spatially divided habitat fragments, but connected via dispersal across less adequate habitat (Hanski, 1991). Understanding how patchy habitats and fragmentation affect survival, dispersal, and growth within metapopulations is critical to their conservation. Theoretical models make many assumptions about growth and dispersal to predict metapopulation dynamics (Amarasekare, 1998; Parker, 1999; Hanski & Ovaskainen, 2000). To effectively use such models to prioritize conservation efforts, we must determine which are best supported by data using experimental tests of their predictions (Kareiva, 1989; Holyoak & Lawler, 2005).

Metapopulation dynamics are affected by factors beyond the within-patch survival and growth of constituent subpopulations. A growing body of literature links classic metapopulation theory with graph, or network, theory. In the latter framework, the metapopulation's subpopulations occupy habitat fragments, which are nodes in a graph, and dispersal between any two fragments can be represented by a graph edge (Urban, Minor, Treml, & Schick, 2009). Using this network-theoretic approach, we can use graph analytic metrics such as degree distributions and spanning trees to better describe metapopulations. One such metric is network heterogeneity, which can range from entirely homogeneous, in which all subpopulations are equally connected to their neighbors, to strongly heterogeneous, as, for example, when most subpopulations are connected to only one or two neighbors while a few "hub" subpopulations are more highly connected (Dale & Fortin, 2010; Gilarranz & Bascompte, 2012). In other words, the connectivity degree of each subpopulation, or the number of dispersal corridors by which it is connected to the network is uniform in a homogeneous metapopulation, but right-skewed in a more heterogeneous metapopulation (Urban & Keitt, 2001; Molofsky & Ferdy, 2005; Artzy-Randrup & Stone, 2010).

Interpreting metapopulation dynamics through the lens of such network-theoretic metrics allows us to draw parallels among diverse types of networks, both biological and non-biological. For example, empirical work in systems as diverse as the World Wide Web (Albert, Jeong, & Barabási, 2000) and stream systems (Fagan, 2002) supports models suggesting that heterogeneous networks are more robust to local failure than their more homogeneous counterparts.

Theoretical modelling by Albert and colleagues (2000) demonstrated that heterogeneous networks are more robust to failures and that such robustness cannot be explained simply by path redundancy. Rather, heterogeneous networks have a smaller diameter, or average path length between any two nodes, and this interconnectedness allows information, or in a metapopulation, dispersing individuals, to cross the network more quickly. And a heterogeneous network has so few nodes that are highly connected that a random local failure is more likely to happen at a poorly connected node. Thus, the remaining nodes in such a network can still communicate with

each other, which makes the network less likely to experience global failure than would a more homogeneous network experiencing a similar level of local failure.

In metapopulations, a subpopulation can be rescued from extinction by migration from neighboring populations, and such rescues can increase the probability that the metapopulation will persist through time (Brown & Kodric-Brown, 1977). Subpopulation connectedness can influence how important this rescue effect is to metapopulation persistence. Because highly connected subpopulations are more likely to be rescued by migration from neighbors, a metapopulation containing many highly connected subpopulations is expected to have a greater rate of recovery and, therefore, a higher probability of persistence than a metapopulation with fewer highly connected subpopulations (Eriksson, Elías-Wolff, Mehlig, & Manica, 2014). However, whether the arrangement of dispersal corridors in space can itself affect the recovery of the metapopulation has never been explored empirically, despite the fact that a deeper understanding of such dynamics could provide critical conservation information.

In addition, the size of the extinction, or percentage of subpopulations that go extinct, could interact with the effects of corridor arrangement on metapopulation recovery. For example, Albert and colleagues found that as the fraction of nodes lost in a network rose, the diameter of the network rose slowly in more homogeneous networks. However, in heterogeneous networks, the diameter of the network was largely unaffected when nodes were lost at random, but when highly connected nodes were targeted for removal, the diameter of the network increased rapidly as the fraction of nodes lost increased.

Here, I used the network-theoretic concept of heterogeneity to characterize dispersal corridor spatial distributions of experimental bacterial metapopulations and tested the effect of that heterogeneity on recovery following subpopulation extinctions. I predicted that metapopulations with heterogeneous corridor arrangements, compared to those with homogeneous arrangements, would recover faster from subpopulation extinction events of all sizes. However, at higher extinction sizes, I predicted the difference in recovery rate between homogeneous and heterogeneous metapopulations would be larger.

Methods

To compare the rate of recolonization and recovery following subpopulation extinction between metapopulations with different degrees of network heterogeneity in their dispersal corridors I conducted a fully crossed experiment with two treatments: corridor arrangement and extinction level. Corridor arrangement treatments were produced in Metapopulation Microcosm Plates (MMPs) with 96 wells, 95 of which were connected by 176 corridors. One unconnected well served as an uninoculated control for cross-contamination. The three corridor arrangements were: homogeneous, heterogeneous, and variable (Figure 2.1). In the homogeneous arrangement, wells were connected in an even lattice arrangement by 4.0 mm corridors. In the heterogeneous arrangement, wells were connected by corridors of variable lengths. Well connectivities followed a right-skewed distribution such that a few wells were highly connected whereas most were connected to only one or two other wells. In the variable arrangement, the wells were connected in the even lattice arrangement of the homogeneous treatment with the distribution of corridor lengths matching the heterogeneous treatment. All MMPs were assembled according to the general instructions described in chapter 1.

The extinction levels were 10% (10 wells) extinct, 50% (48 wells) extinct, 90% (86 wells) extinct, and a 0% no extinction control. In each run of the experiment (Figure 2.2), parent plates of each corridor arrangement treatment level were needle inoculated in every well with *Pseudomonas syringae* pv. *syringae* B728a expressing gfp from an overnight culture at a concentration of 1.0-1.7 x 10^6 CFU/mL. The needles used for all inoculations in this experiment transferred) 0.651 ± 0.347 (SD) µL volume, meaning that each well of the parent plates began with approximately 2.2-12.1 x 10^3 CFU/mL in each well. Parent plates were incubated at 22°C for 48 hours, then subsampled into daughter plates with identical corridor arrangements using a plate replicator from which a random subset of pins had been removed (e.g. to create the 10% treatment, 10 pins were removed from the plate replicator). The identities of the extinct wells were chosen by sorting the wells of the heterogeneous corridor arrangement by their degree (number of neighbors) and choosing a random subset of each degree, approximately in proportion with the overall degree distribution of the heterogeneous treatment (Figure 2.3). The same well identities were extinguished in every corridor arrangement treatment, such that if well B6 was chosen as an extinct well, it was made to go extinct in all plates. Each daughter plate was incubated at 22°C for 156 hours and its fluorescence was measured in a microplate reader every 12 hours. The full experiment was run six times for a total of six replicates (plates) of each treatment combination. All uninoculated controls remained sterile.

As a measurement of recovery following extinction, I calculated the deviation of each well on each treatment plate from the corresponding well on its control plate (the 0% extinction plate subsampled from the same parent plate), normalized to the control value and starting inoculum concentration, using the following formula:

$$Deviation\ from\ Control = ((Fluor_T/Start)-(Fluor_C/Start))/(Fluor_C/Start)$$

where $Fluor_T$ is the fluorescence of the treatment well, $Fluor_C$ is the fluorescence of the corresponding control well, and *Start* is the concentration of the culture from which the parent plate was inoculated (Figures 2.4 and 2.5). I used this quantity to calculate three recovery metrics:

1) Time to Begin Recovery Phase – I defined the recovery phase of each plate's time series as the portion during which the change in deviation from the control was positive (i.e. the treatment plate was becoming more similar to the control). I calculated the time at which this recovery phase began for each plate.

2) Maximum Rate of Recovery – I fit each recovery phase with linear, quadratic, cubic, and quartic regressions and chose the model which fit the data best using AICc model selection. I then found the derivative of each best fit model and used it to calculate the maximum rate of recovery during the recovery phase for each treatment.

3) Time to Recovery – Using a planned contrast at each time step, I defined the time to recovery as the first time period at which there was no significant difference between the treatment and control.

I calculated all three metrics for each combination of corridor arrangement and extinction level both for the mean of all subpopulations and for extinction subpopulations only. To assess

whether variability in re-colonization affected the recovery of the metapopulations, I also calculated the standard deviation of Deviation of Control of the wells of each plate.

Finally, with all subpopulations, I fit several multiple polynomial linear mixed effects models using Deviation from Control after 36 hours (to include only time points after recovery had begun for all plates) as the response variable and including run of the experiment as a random effect. Hours post-extinction, hours post-extinction squared, and hours post-extinction cubed were included as explanatory variables in all models. One or more of the following were also included in each model as explanatory variables: corridor arrangement, extinction level, and the interaction between corridor arrangement and extinction level. I chose the model with the lowest AIC_c value as the best fit model. I repeated this procedure with extinct subpopulations only. I assessed homogeneity of variance and normality of residuals by plotting the residuals. All analyses were performed in R (R Core Team, 2016).

In all runs of this experiment, MMPs were filled with Luria-Bertani liquid medium (LB; Cold Spring Harbor Protocols, 2006) containing 40 µg/mL nitrofurantoin and 15 µg/mL tetracycline to select against loss of mutant plasmids. This experiment was performed using wild type *Pseudomonas syringae* pv. *syringae* B728a containing the *pkln42gfp* plasmid, which constitutively expresses *gfp* (Dulla & Lindow, 2008). This strain is motile and doubles approximately every 3 h at 15°C in this set-up. This *Pseudomonas* strain was generously provided to me by the Lindow Lab, UC Berkeley.

Results

Time to Begin Recovery Phase

Apart from the homogeneous corridor 10% extinction treatment combination, which grew faster than the control during all periods, all 10% and 50% extinction metapopulations began to recover (approach their controls) after 24 hours. All 90% extinction metapopulations began to recover after 36 hours (Table 2.1a). All extinct subpopulations in the 10% and 50% extinction metapopulations began to recover after 24 hours and all extinct subpopulations in the 90% extinction metapopulations began to recover after 36 hours (Table 2.1b).

In general, the metapopulations experiencing 10% extinction recovered to the highest mean subpopulation sizes (relative to their controls), 50% extinction had intermediate subpopulation sizes, and the 90% extinction treatment had the lowest subpopulations sizes. Within the 10% extinction treatment, metapopulations with homogeneous corridors reached the highest subpopulations sizes, while in the 50% extinction treatment, metapopulations with heterogeneous corridors were highest (Figure 2.6a). The patterns were the same amongst the extinct wells (Figure 2.6b). Standard deviation of the "deviation from control" response variable was highest in the 90% extinction treatment, intermediate in the 50% extinction treatment, and lowest in the 10% extinction treatment. Within the 10% extinction treatment, the standard deviation was highest in the variable corridor metapopulations, intermediate in heterogeneous corridors, and lowest in homogeneous. Within the 50% and 90% extinction treatments, the standard deviation was highest in heterogeneous metapopulations, intermediate in variable metapopulations, and lowest in homogeneous (Figure 2.7a). The patterns were generally the same amongst extinct wells, with the exception of the heterogeneous 50% extinction treatment combination, which had the highest standard deviation (Figure 2.7b).

Maximum Rate of Recovery

All recovery phase trajectories were fit best (had the lowest AIC_c value) by a quadratic or cubic model. The mean recoveries of all subpopulations were fit best by cubic models for all treatment combinations except 10% and 50% extinction in homogeneous corridors and 10% extinction in variable corridors, which were fit best by quadratic models (Table 2.2a). The recoveries of extinct subpopulations were fit best by cubic models for all treatment combinations except 10% extinction in homogeneous and heterogeneous corridors and 50% extinction in variable corridors; those exceptions were fit best by quadratic models (Table 2.2b).

For the mean recovery of all subpopulations, the maximum rate of recovery in metapopulations with heterogeneous corridors was highest in the 50% extinction treatment, while in metapopulations with homogeneous and variable corridors the rate was highest in the 90% extinction treatment. At all extinction levels, recovery was fastest in metapopulations with heterogeneous corridors (Figure 2.8a). Recovery amongst extinct subpopulations in metapopulations with heterogeneous corridors was fastest in the 50% extinction treatment. In metapopulations with homogeneous or variable corridors, recovery was fastest in the 90% extinction treatment. At all extinction levels, recovery of extinct wells was fastest in metapopulations with heterogeneous corridor arrangements (Figure 2.8b).

Time to Recovery

In the 10% extinction treatment, metapopulations with a heterogeneous corridor arrangement became statistically indistinguishable from their controls after 60 hours, whereas homogeneous metapopulations took only 12 hours, and metapopulations with the variable corridor arrangement took 36 hours. In the 50% extinction treatment, heterogeneous metapopulations still took 60 hours to recover to the control condition, whereas homogeneous metapopulations took 108 hours, and metapopulations with the variable corridor arrangement took 72 hours. No metapopulations recovered to the control condition following a 90% extinction (Figure 2.9a).

In metapopulations with the heterogeneous corridor arrangement, extinct subpopulations took an average of 72 hours to recover from both 10% and 50% extinction treatments. In metapopulations with the homogeneous corridor arrangement, extinct subpopulations took 36 hours and 144 hours to recover from 10% and 50% extinction treatments, respectively. On metapopulations with variable corridor arrangements, extinct subpopulations took 48 hours and 120 hours to recover from 10% and 50% extinction treatments, respectively (Figure 2.9b).

Polynomial Regression

All polynomial regression models of all subpopulation recoveries containing an interaction term fit the data equally well and better than all models that did not contain an interaction term (Table 2.3a). Tukey's Honestly Significant Difference showed that all corridor arrangement by extinction level treatment combinations were significantly different from all others ($p_{HSD} < 0.001$) except 50% extinction in homogeneous corridors from 50% extinction in heterogeneous corridors ($p_{HSD} = 0.149$), 90% extinction in variable corridors from 90% extinction in homogeneous corridors ($p_{HSD} = 0.102$), and 90% extinction in variable corridors

from 90% extinction in heterogeneous corridors ($p_{HSD} = 0.173$). The same pattern was true among models of extinct subpopulation recoveries (Table 2.3b).

Discussion

In this experiment, metapopulations with heterogeneous corridor arrangements had a faster maximum rate of recovery from all levels of extinction than those with other corridor arrangements, which matched my predictions. However, that greater maximum speed translated to a shorter absolute time to recovery only in the 50% extinction treatment. Following the 10% extinction treatment, metapopulations with homogeneous corridor arrangements recovered to their control condition in a shorter absolute time than did the heterogeneous metapopulations. This may be because when extinctions occur in a random subset of subpopulations, few are likely to occur in adjacent subpopulations, and therefore an extinct subpopulation is almost certain to be adjacent to an occupied subpopulation, which leads to rapid recolonization. In the homogeneous treatment, that extinct subpopulation is always only a short distance from its occupied neighbor, again leading to rapid recolonization. However, in the heterogeneous treatment, bacteria may have to travel down a longer corridor, despite being only a short straight-line distance from the adjacent extinct subpopulation. Most work on network heterogeneity, including that of Albert and colleagues (2000), considers unweighted networks, in which all edges are equal. In metapopulation ecology, however, the edges of spatial networks are weighted. Assuming that the time it takes an individual organism to travel from one patch to another is a function of the length of corridor between the patches, each dispersal corridor could be assigned a weight proportional to its length (Urban et al., 2009). Therefore, predictions that heterogeneous networks will be the most robust to node failure in unweighted networks may not translate perfectly to recovery dynamics in weighted networks.

To further examine this idea, we can compare the recovery of metapopulations with the variable corridor arrangement to that of metapopulations with heterogeneous and homogeneous corridor arrangements. The variable treatment had a corridor arrangement in a regular lattice which matched that of the homogeneous treatment, but with a distribution of corridor lengths which matched that of the heterogeneous treatment. If the differences in recovery rate and time between the heterogeneous and homogeneous treatments can be explained primarily by the addition of longer dispersal corridors in the heterogeneous treatment, then recovery in the variable treatment should be similar to that of the heterogeneous treatment. If instead those differences are due primarily to differences in the corridor arrangement, then recovery in the variable treatment should be more similar to that of the homogeneous treatment. With one exception, both the rates of recovery and the absolute times to recovery of the variable treatment are intermediate between those of the heterogeneous and homogeneous treatments at every extinction level. The exception is that the recovery rate of all subpopulations in the 10% extinction treatment was slightly lower in metapopulations with a variable corridor arrangement than in those with either of the other corridor treatments. This result suggests that, while some of the difference between the heterogeneous and homogeneous treatments can be attributed to their differences in corridor length, a portion can also be attributed directly to differences in their network heterogeneity.

In standard deviation too, the variable corridor treatment is intermediate between the homogeneous corridors, which had the lowest variation in deviation from the control, and heterogeneous corridors, which had the highest variation, except for at the 10% extinction level when the variable treatment slightly exceeded the heterogeneous in variability. Here again, it is possible that the difference in corridor length between the homogeneous and heterogeneous treatments contributes to the difference in their variability, because in order for an extinct subpopulation to be recolonized individuals must travel from an occupied subpopulation. In a homogeneous metapopulation that distance is always the same, while in a heterogeneous metapopulation the distance, and therefore the time for an extinct subpopulation to be recolonized, will vary. If this variability in corridor length and travel time was the principal driver of differences in recovery between the heterogeneous and homogeneous corridor treatments, we would expect the standard deviation of the variable treatment to match that of the heterogeneous treatment. Its position intermediate between the heterogeneous and homogeneous treatments suggests again that while corridor length contributes to this difference, network heterogeneity also makes a contribution.

While it is unfortunate that none of the 90% extinction treatments recovered fully to the level of their controls within the timeframe of the experiments, we can consider their rates of recovery. In the 10% extinction treatment, despite the fact that the heterogeneous corridor metapopulation has the highest rate of recovery, the homogeneous corridor metapopulation recovers in the shortest absolute time because it begins its recovery sooner and never deviates as far from its control as does the heterogeneous metapopulation. In the 50% extinction treatment, the heterogeneous metapopulation again deviates the farthest from its own control, but the combination of beginning its recovery at the same time as the other corridor arrangements and having a faster rate of recovery, leads to a shorter absolute time to recovery. In the 90% extinction treatment, by comparison, the heterogeneous metapopulation continues its pattern of deviating the farthest from its control, although the difference between the greatest deviation of the homogeneous and heterogeneous treatments is smaller than in the other extinction treatments. The heterogeneous metapopulation also has the highest rate of recovery in the 90% extinction treatment, although it is lower than the rate of recovery of the heterogeneous metapopulation in the 50% extinction treatment and the difference between the rates of the heterogeneous and homogeneous metapopulations in the 90% extinction treatment is much small that in the 50% extinction treatment. This suggests that while the heterogeneous metapopulation had the shortest time to recovery in the 50% extinction treatment, that pattern might not have continued in the 90% extinction treatments, had they had the time and resources to recover to control levels. This switch in order of recovery from homogeneous soonest in the 10% extinction treatment, to heterogeneous soonest in the 50% extinction treatment, and possibly back again in the 90% extinction treatment, may explain why the data was fit equally well by all polynomial models that contained a corridor arrangement by extinction level interaction term, meaning that all recovery trajectories were different from each other with no clear trends in the main effects of corridor arrangement or extinction level.

The effects of rescue by recolonization from neighboring subpopulations are important for long-term metapopulation persistence. For example, and Gilarranz and Bascompte (2012) used variations of the Hanski and Ovaskainen (2000) and Levins (1969) models to predict that higher network heterogeneity in metapopulations will lead to a higher proportion of occupied patches, but that that pattern will reverse at low extinction-to-colonization ratios. Highly connected subpopulations are likely to be recolonized more quickly by their occupied neighbors.

But whether that higher rate of recolonization translates into faster recovery of the metapopulation has not been explored empirically. In this experiment, extinct subpopulations were recolonized fastest in metapopulations with heterogeneous corridors, and that recolonization led to faster recovery of the metapopulations themselves.

Understanding this type of interplay between habitat fragmentation, connectivity, and metapopulation dynamics is critical to conservation. For example, Fortuna and colleagues (Fortuna, Gómez-Rodríguez, & Bascompte, 2006) found that variation in the wetness of the environment affected the availability of dispersal corridors for amphibians between temporary ponds, but that because of underlying connectivity amongst the ponds, amphibian dispersal was unlikely to be dramatically affected by loss of individual ponds. Similarly, Cowley, Johnson, and Pocock (2015) used network-theoretic metrics to model the spread of oak processionary moths through oak woodlands and identify the most important patches or 'pinch points' of invasion. Their results suggested that the patches they identified would be most critical for conservation interventions to prevent invasion spread.

A better understanding of how the spatial arrangement of dispersal corridors on the landscape might lead to different recovery outcomes depending on the size of the of the extinction event could be useful in guiding efforts to plan the positions of artificial dispersal corridors between habitat patches or preserve existing corridors. This experiment demonstrates that heterogeneous connectivity among subpopulations can lead to faster recovery following subpopulation extinction, but that greater speed of recovery may not always translate to a shorter absolute time to recovery.

Table 2.1. Hours to beginning of recovery phase for each corridor arrangement by extinction level treatment combination for a) all subpopulations and b) extinct subpopulations only (no variation between replicates).

a)

Corridor Arrangement	Extinction Level		
	10%	50%	90%
Heterogeneous	24	24	36
Homogeneous	0	24	36
Variable	24	24	36

b)

Corridor Arrangement	Extinction Level		
	10%	50%	90%
Heterogeneous	24	24	36
Homogeneous	24	24	36
Variable	24	24	36

Table 2.2. Akaike's Information Criterion (corrected) for quadratic, cubic, and quartic fits of deviation from control (response variable) to hours post-extinction (explanatory variable) for each corridor arrangement by extinction level treatment combination for a) all subpopulations and b) extinct subpopulations only. Asterisks indicate lowest AIC_c value for each treatment combination.

a)

Corridor Arrangement	Model	Extinction Level 10%	50%	90%
Heterogeneous	Linear	-39.4617	-22.0386	-24.9291
	Quadratic	-53.7318	-39.2041	-44.7481
	Cubic	-59.7019 *	-65.2271 *	-56.6741 *
	Quartic	-51.2729	-58.1565	-48.1174
Homogeneous	Linear	-48.2980	-43.9183	-39.4198
	Quadratic	-49.3780 *	-47.0253 *	-60.1964
	Cubic	-46.6867	-43.4258	-67.6496 *
	Quartic	-42.4921	-36.5383	-58.0035
Variable	Linear	-63.9602	-31.3703	-29.7178
	Quadratic	-64.6027 *	-46.8633	-42.8304
	Cubic	-58.9160	-63.3159 *	-49.0503 *
	Quartic	-54.6492	-59.3679	-38.5186

b)

Corridor Arrangement	Model	Extinction Level 10%	50%	90%
Heterogeneous	Linear	-22.6111	-16.9759	-22.6932
	Quadratic	-37.4289 *	-37.9181	-43.1829
	Cubic	-36.9965	-39.8914 *	-58.4686 *
	Quartic	-34.0553	-39.1637	-49.7853
Homogeneous	Linear	-37.8690	-37.1679	-35.4313
	Quadratic	-44.2283 *	-51.3898	-54.1195
	Cubic	-42.1109	-51.5477 *	-63.7529 *
	Quartic	-35.3900	-43.0327	-55.1379
Variable	Linear	-36.2196	-26.3050	-28.4031
	Quadratic	-53.7085	-45.9971 *	-42.7694
	Cubic	-53.7487 *	-45.4415	-47.7391 *
	Quartic	-49.0770	-38.8143	-37.0167

Table 2.3. Akaike's Information Criterion (corrected) for multiple polynomial regression fits of deviation from control (response variable), linear, squared, and cubic terms for hours post-extinction (HPE), and corridor arrangement (Corr), extinction level (Ext), and corridor arrangement by extinction level interaction (Corr:Ext) for a) all subpopulations and b) extinct subpopulations only. Asterisks indicate best-fit models.

a)

Model (Right-hand side)	Parameters	Log likelihood	AIC_c
HPE + HPE^2 + HPE^3 + Corr + Ext + Corr:Ext	14	61.68	-95.34 *
HPE + HPE^2 + HPE^3 + Corr + Ext	10	-132.78	285.56
HPE + HPE^2 + HPE^3 + Corr	8	-11263.56	22543.12
HPE + HPE^2 + HPE^3 + Ext	8	-269.26	554.53
HPE + HPE^2 + HPE^3 + Corr + Corr:Ext	14	61.68	-95.34 *
HPE + HPE^2 + HPE^3 + Ext + Corr:Ext	14	61.68	-95.34 *
HPE + HPE^2 + HPE^3 + Corr:Ext	14	61.68	-95.34 *
HPE + HPE^2 + HPE^3	6	-11355.62	22723.25

b)

Model (Right-hand side)	Parameters	Log likelihood	AIC_c
HPE + HPE^2 + HPE^3 + Corr + Ext + Corr:Ext	14	-2070.66	4169.34 *
HPE + HPE^2 + HPE^3 + Corr + Ext	10	-2158.35	4336.70
HPE + HPE^2 + HPE^3 + Corr	8	-5564.44	11144.88
HPE + HPE^2 + HPE^3 + Ext	8	-2200.43	4416.86
HPE + HPE^2 + HPE^3 + Corr + Corr:Ext	14	-2070.66	4169.34 *
HPE + HPE^2 + HPE^3 + Ext + Corr:Ext	14	-2070.66	4169.34 *
HPE + HPE^2 + HPE^3 + Corr:Ext	14	-2070.66	4169.34 *
HPE + HPE^2 + HPE^3	6	-5597.59	11207.18

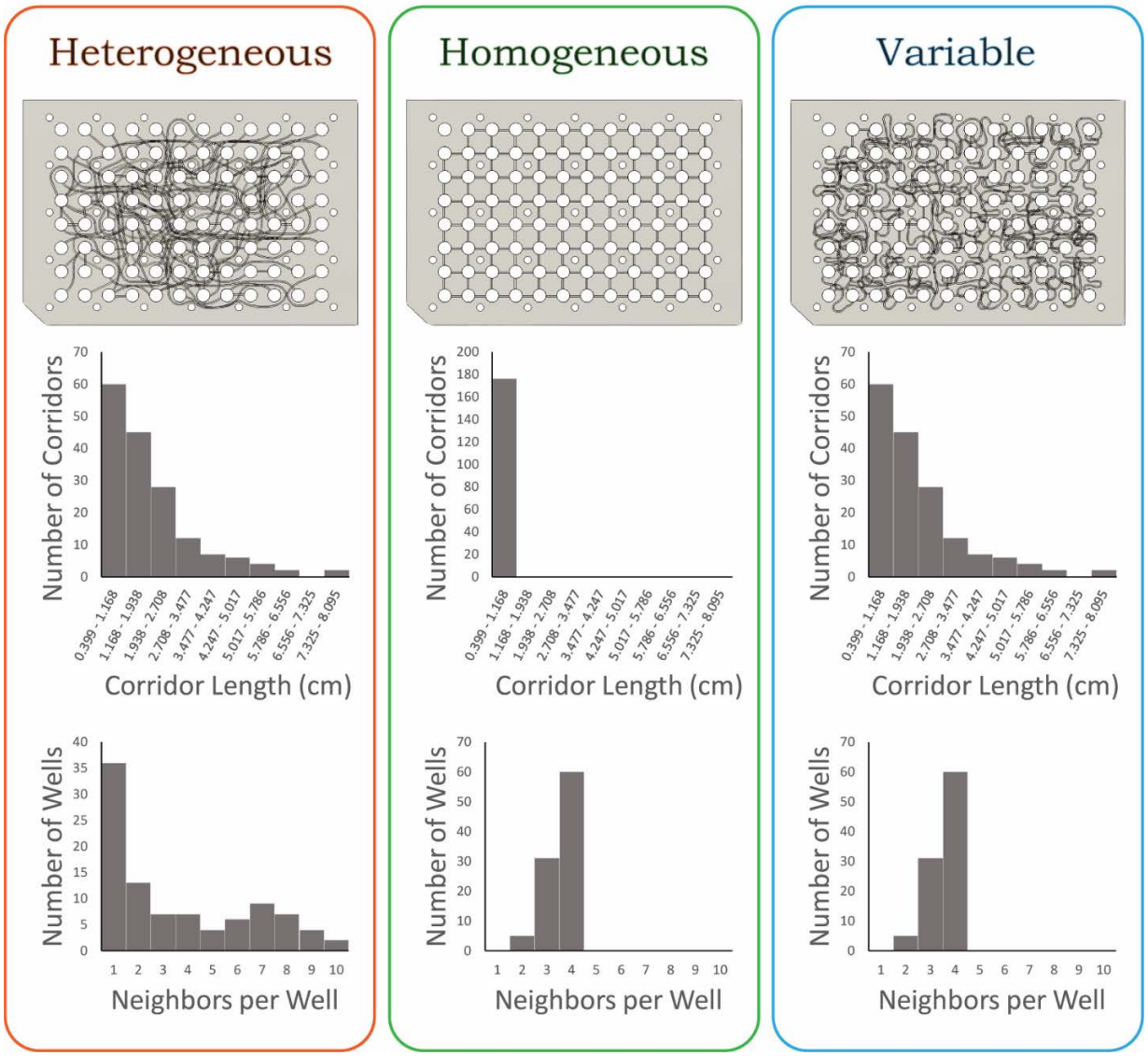

Figure 2.1. Corridor arrangement treatments: diagrams (top), histograms of corridor lengths (middle), histograms of neighbors per subpopulation (bottom).

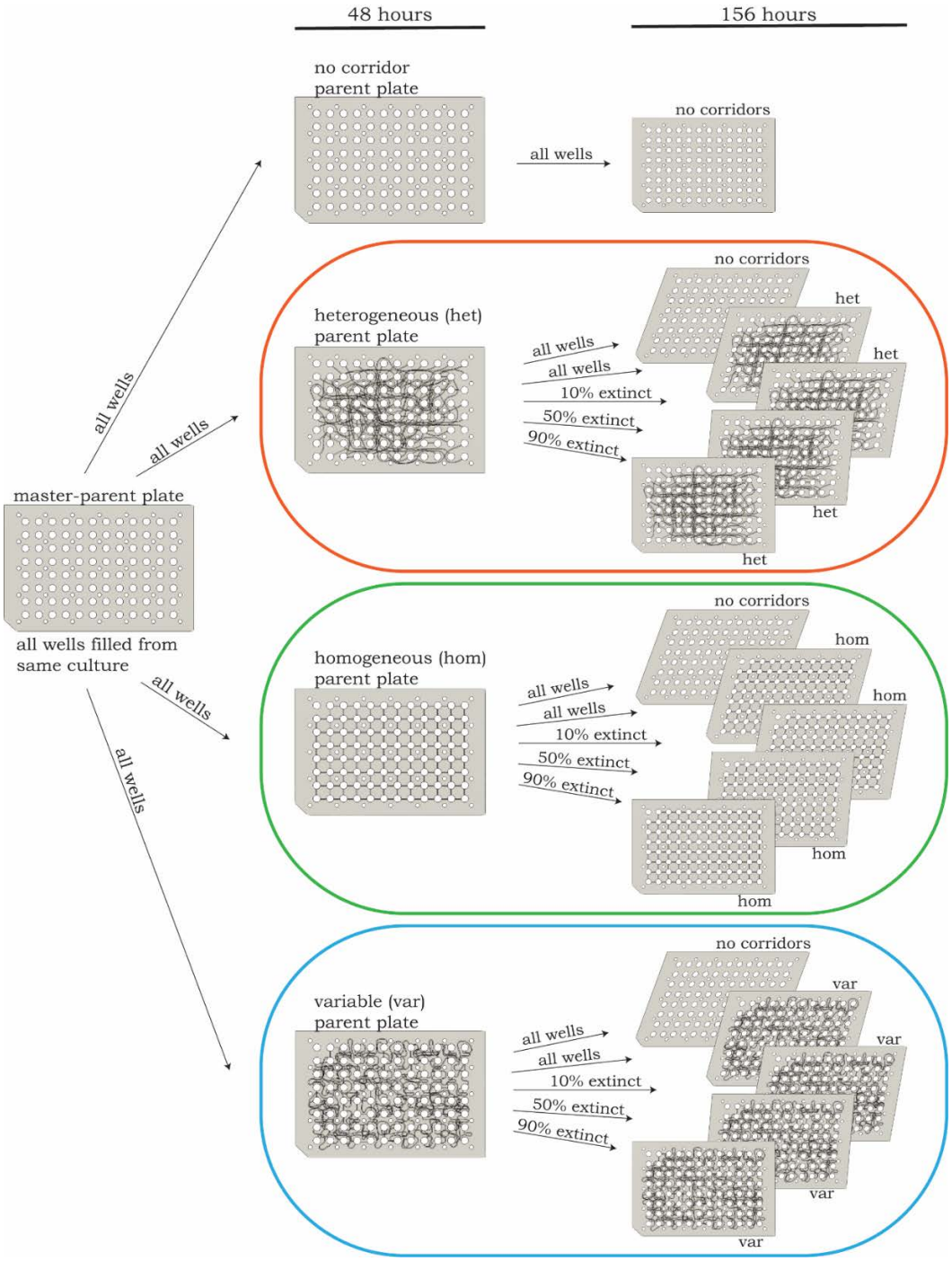

Figure 2.2. Experimental design: For each run of the experiment, all wells of the master-parent plate were filled from an overnight culture of *Pseudomonas syringae*. All wells of the master-parent plate were then sub-sampled into parent plates with homogeneous, heterogeneous, and variable corridor arrangements. These parent plates were incubated at 22℃ for 48 hours. To create the different extinction levels, each parent plate was subsampled to daughter plates with identical corridor arrangements with either 10%, 50%, or 90% of plate replicator pins removed. The daughter plates were incubated 22℃ for 156 hours and each was read in a plate reader every 12 hours.

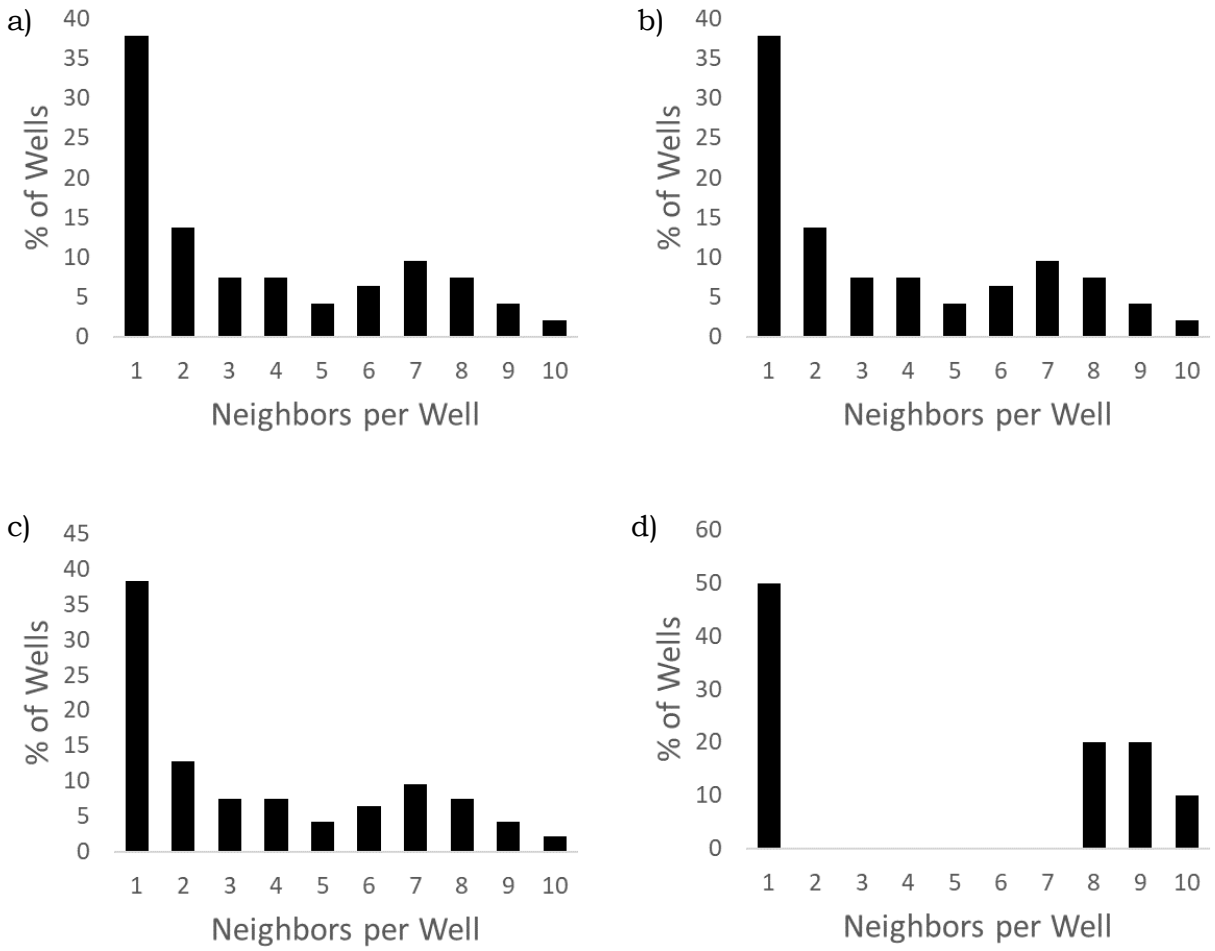

Figure 2.3. Neighbors per subpopulation for a) all subpopulations in heterogeneous corridor arrangement treatment b) extinct subpopulations of 90% extinction level treatment c) extinct subpopulations of 50% extinction level treatment d) extinct subpopulations of 10% extinction level treatment.

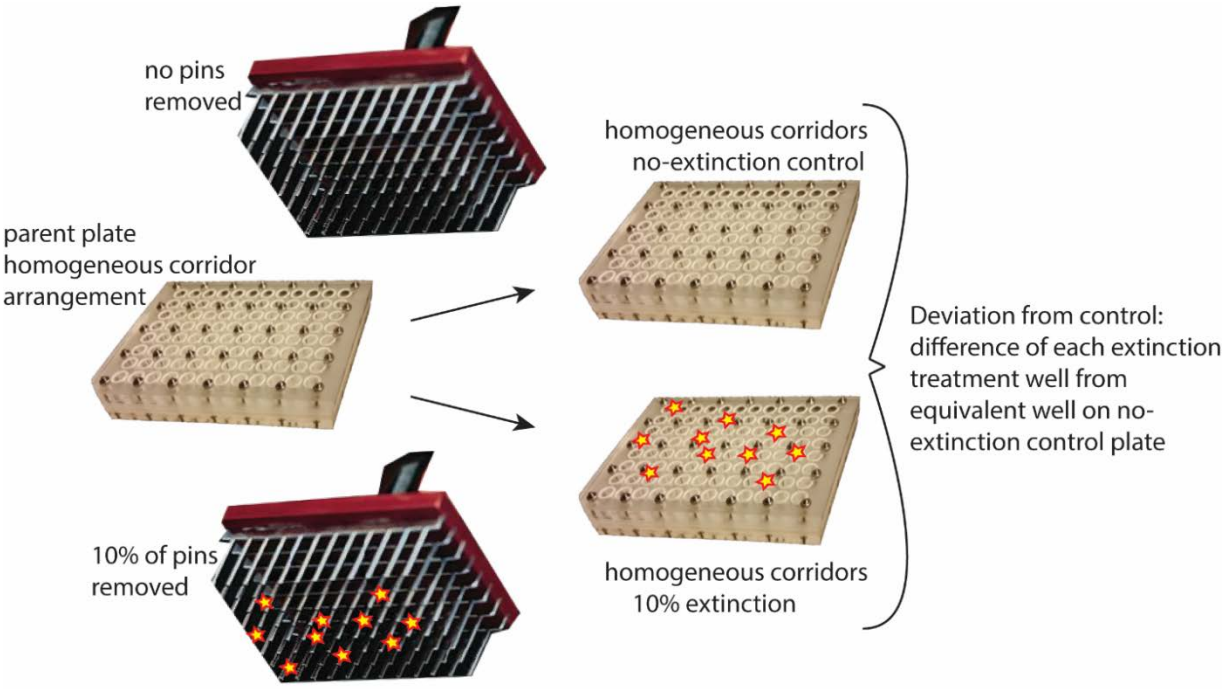

Figure 2.4. Response variable "Deviation from control" was calculated by subtracting fluorescence of each treatment well from the fluorescence of the corresponding well of the no extinction control. In this example, the 10% extinction treatment plate is matched to its no-extinction control plate.

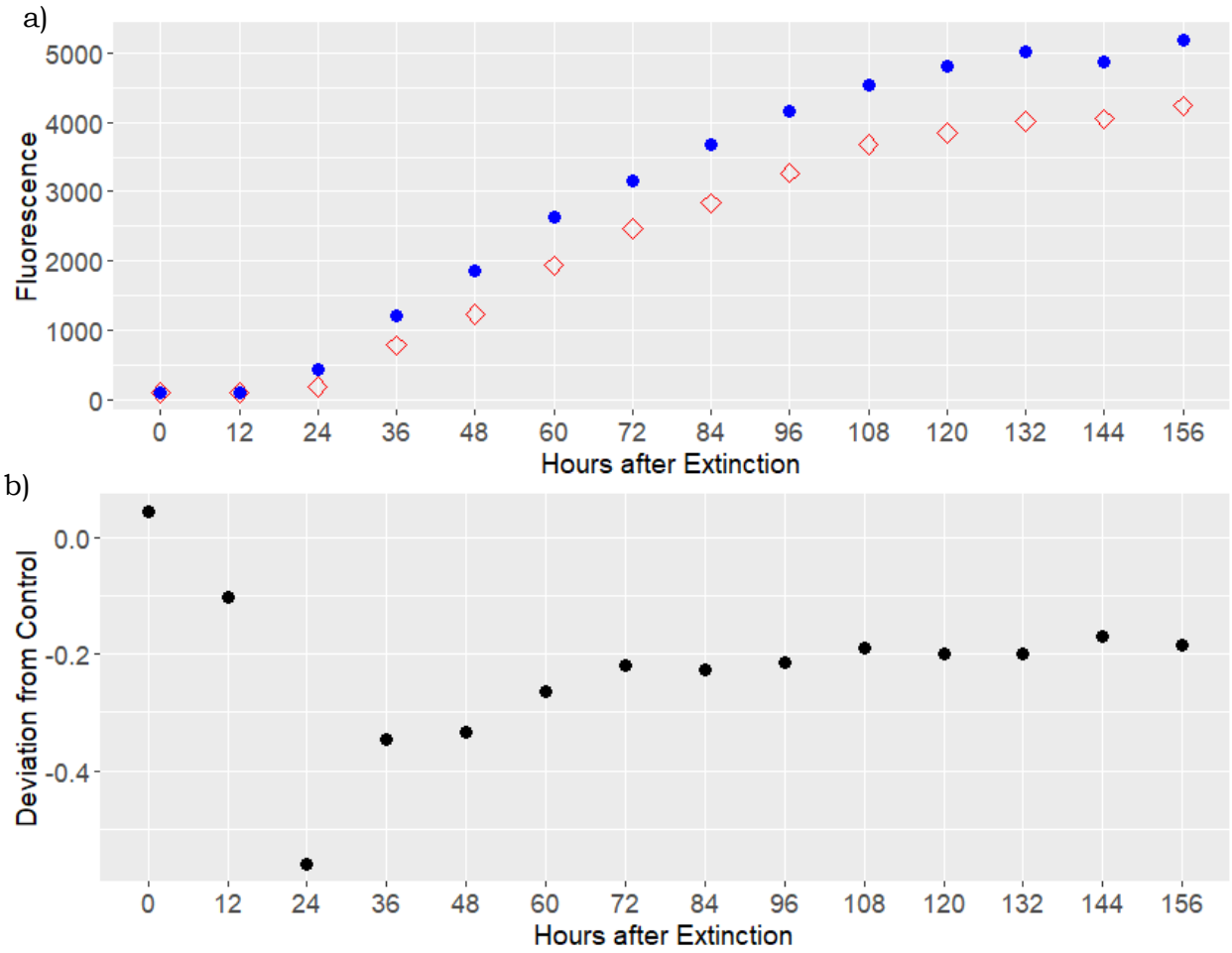

Figure 2.5. Example of raw data and calculation of Deviation from Control a) Time series of fluorescence in well A5 in one pair of plates with heterogeneous corridors, blue circles are well A5 in no-extinction control, red diamonds are well A5 in 10% extinction treatment b) Deviation from Control calculated by subtracting fluorescence in control well (blue circle, panel a) from fluorescence in treatment well (red diamond, panel a), divided by fluorescence in control (blue circle, panel a).

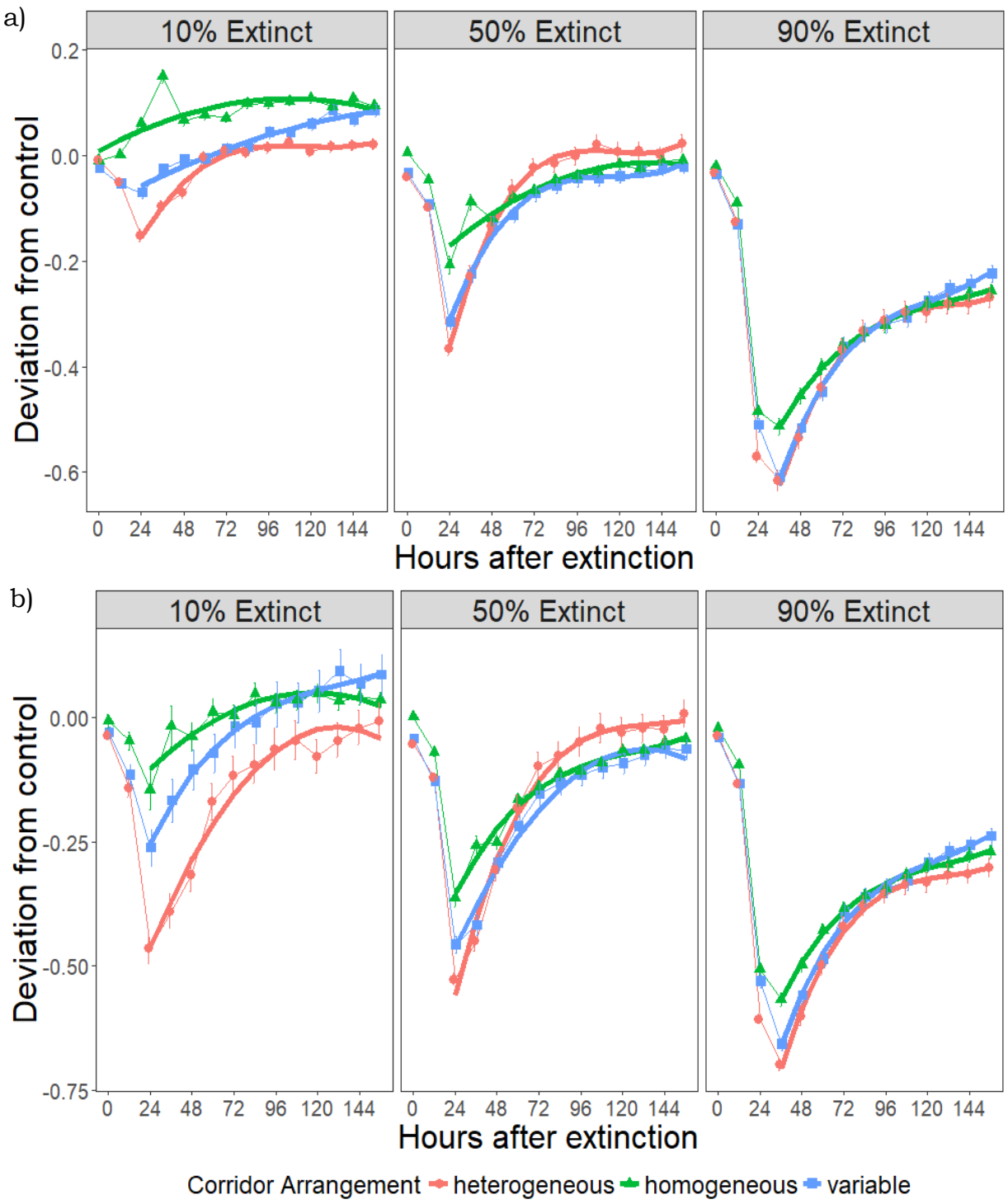

Figure 2.6. Deviation of treatment plates from control plates with heterogeneous, homogeneous, or variable corridor arrangements following 10%, 50%, or 90% extinction of a) all subpopulations or b) extinct subpopulations only. Error bars are standard error of the mean (n=6). Thick lines are best fit lines for each recovery trajectory.

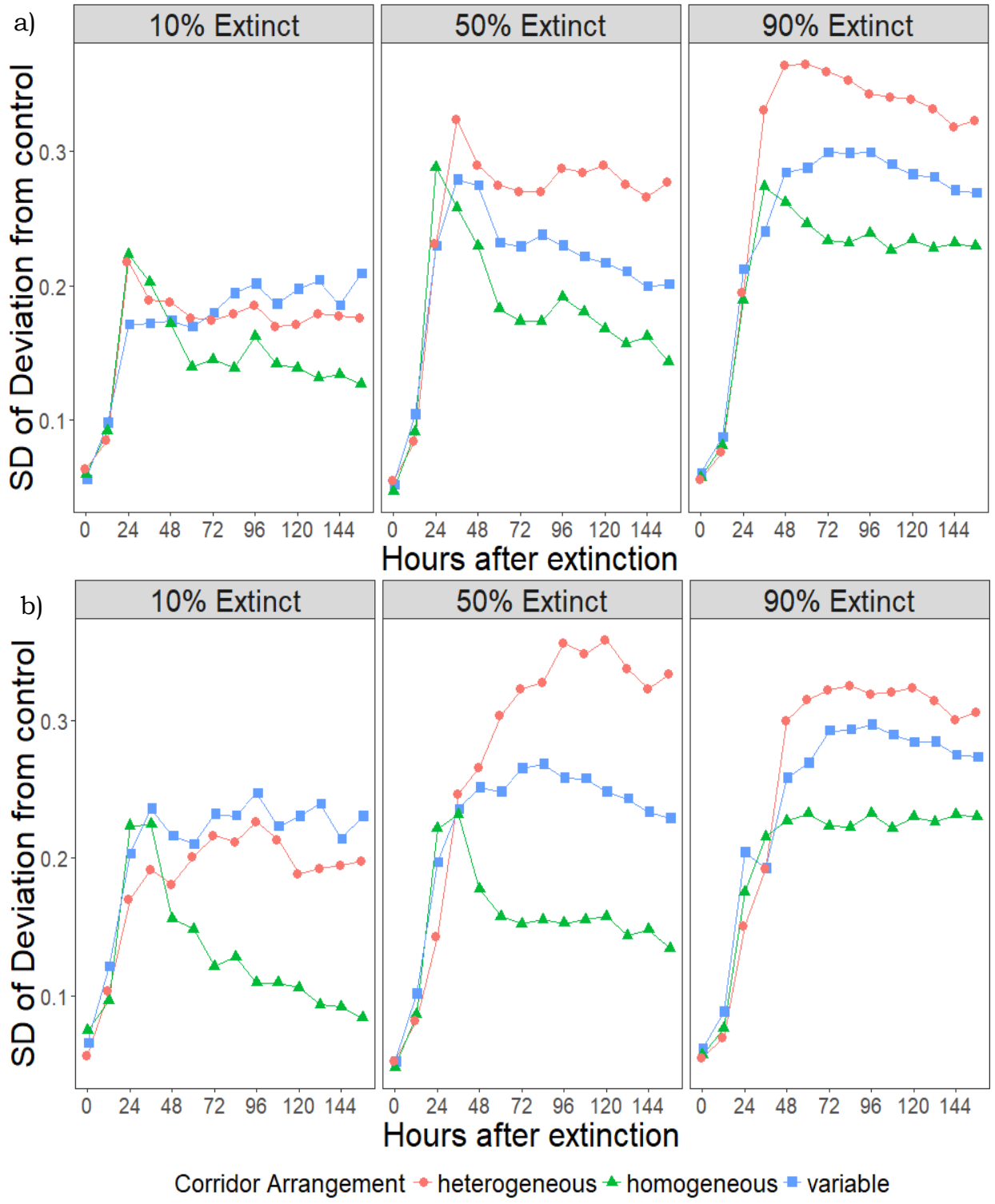

Figure 2.7. Standard deviation of "deviation from control" response variable for heterogeneous, homogeneous, or variable corridor arrangements following 10%, 50%, or 90% extinction of a) all subpopulations or b) extinct subpopulations only.

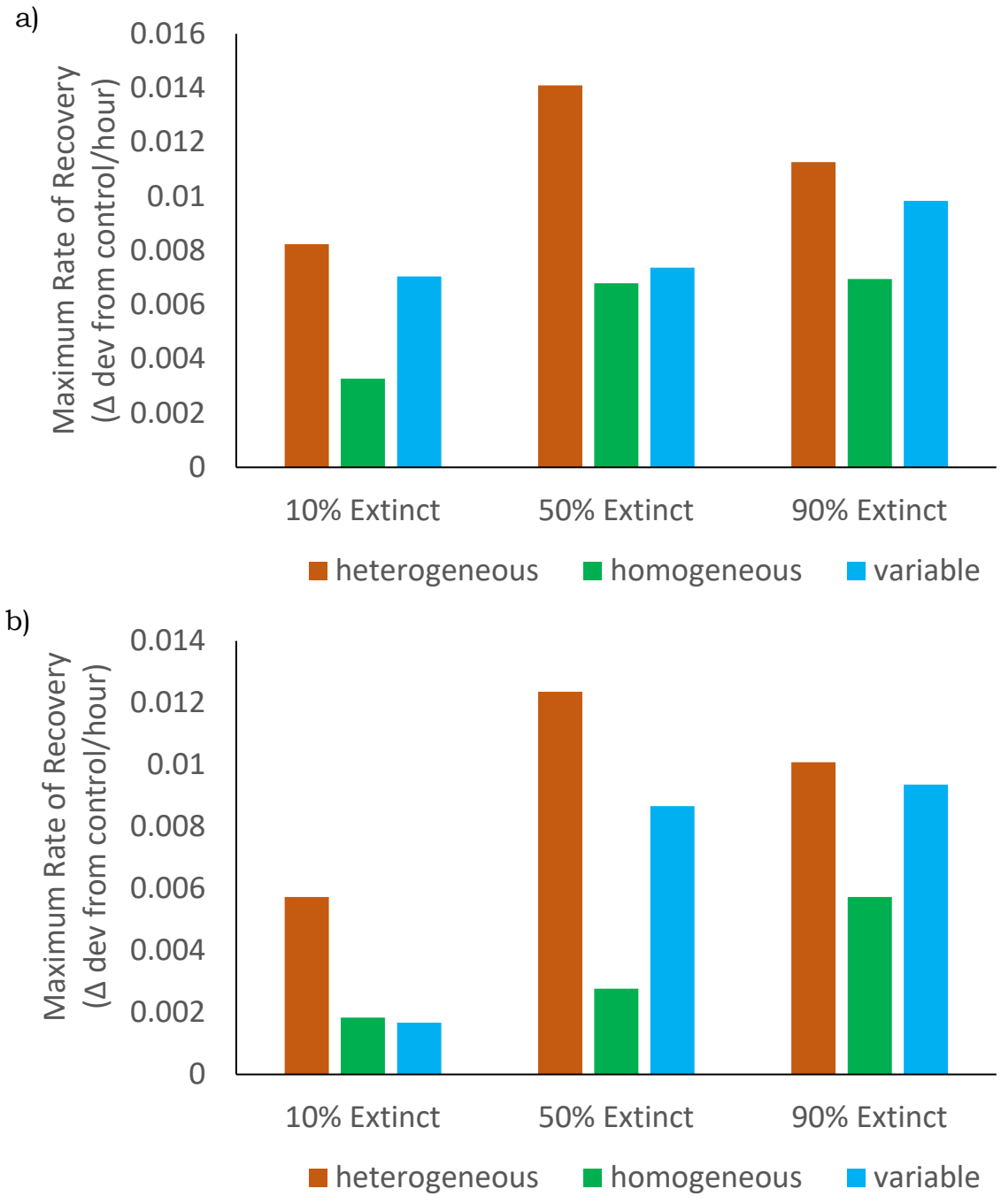

Figure 2.8. Maximum rate of recovery, measured as change in "deviation from control" response variable per hour, for each combination of corridor arrangement and extinction level for a) all subpopulations and b) extinct subpopulations only. This recovery rate maximum was calculated by finding the maximum derivative of the best-fit model [see Table 2.2] during the recovery phase.

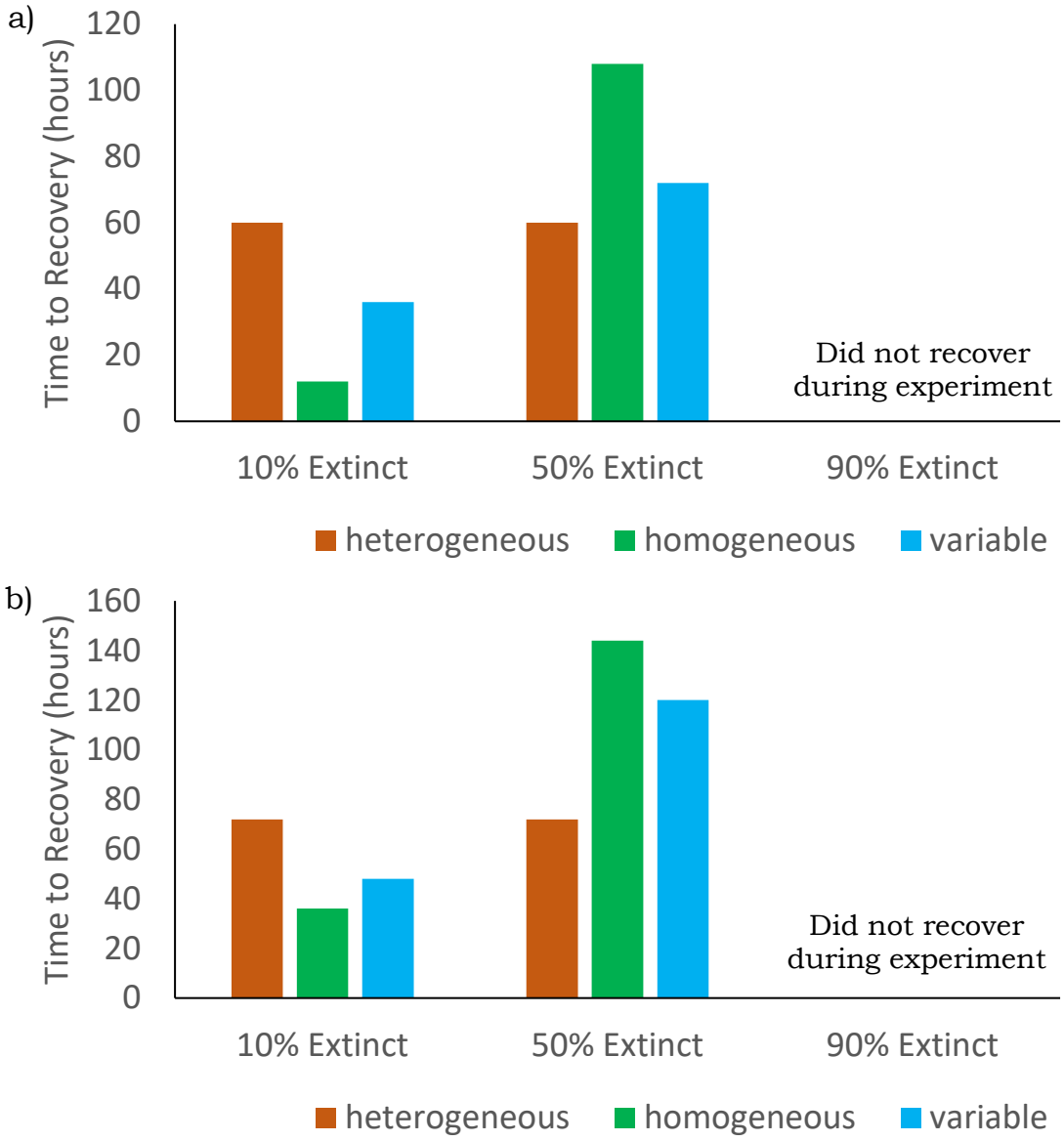

Figure 2.9. Hours to recovery for each corridor arrangement by extinction level treatment combination for a) all subpopulations and b) extinct subpopulations only.

CHAPTER 3

Extinctions in high connectivity subpopulations slow metapopulation recovery rates only after large extinction events

Introduction

Many organisms are sensitive to the habitat through which they are willing or able to disperse and therefore use defined dispersal corridors to move between patches. In such cases, models that explicitly account for the spatial positions of such corridors are needed to understand how these features contribute to metapopulation growth and persistence (Dale & Fortin, 2010). One way to account for these spatial positions is by modeling populations as spatial graphs, using network (also called graph) theory. Doing so provides a host of metrics with which to draw parallels between connected systems of populations in habitat patches and other types of networks, both biological and non-biological (Urban & Keitt, 2001).

When network-theoretic concepts are applied to metapopulations, subpopulations in habitat patches are nodes and dispersal corridors are edges. Each node or subpopulation has a degree, the number of edges that connect it to the network or the number of dispersal corridors that connect it to the metapopulation. One metric to describe these spatial positions is network heterogeneity. In this context, network heterogeneity describes the spatial clustering of edges in a network (Gilarranz & Bascompte, 2012). In a homogeneous network, every node has the same degree and is connected by the same number of edges, which form a perfect lattice. More heterogeneous networks have a few highly connected "hub" nodes of high degree while most other nodes have low degree and are directly attached to only one or two neighbors. Thus, one way to describe the heterogeneity of a network is the probability distribution of node degrees, which is called the network's degree distribution.

Use of network-theoretic metrics such as heterogeneity provides a broader understanding of metapopulations by linking them empirically to other systems, both biological, such as cell metabolic networks and food webs, and non-biological, such as the structure of the internet and social networks (Boitani, Falcucci, Maiorano, & Rondinini, 2007). Albert and colleagues (Albert, Jeong, & Barabási, 2000) found that heterogeneous networks, while very robust to the random loss of nodes, were extremely vulnerable to targeted attacks on highly connected nodes. They simulated the loss of nodes (documents) from a portion of the World Wide Web (WWW), a heterogeneous network, and demonstrated that the WWW would be extremely robust to random loss of nodes, partly because the rarity of highly connected nodes in heterogeneous networks makes them unlikely sites for random losses. However, targeted attacks on highly connected nodes quickly increased the diameter, or average path length between nodes, and increased the probability of global failure of the network. In contrast, less heterogeneous networks did not respond differently to random versus targeted losses. This result suggests that a heterogeneous metapopulation would be more vulnerable to the loss of highly connected subpopulations than it would be to the loss of subpopulations at random, while a more homogeneous metapopulation would show no such difference.

Here, I compared the recovery of bacterial metapopulations with homogeneous and heterogeneous corridor arrangements following small, medium, and large extinction events in either low or high connectivity subpopulations. I predicted that metapopulations with heterogeneous corridor arrangements would recover fastest from the loss of low connectivity subpopulations regardless of the size of the extinction event, while those with homogeneous corridor arrangements would show no difference in their responses to high and low connectivity extinction events.

Methods

Experimental Design

To test my hypotheses, I conducted a fully crossed experiment with three treatments: corridor arrangement, extinction level, and extinction connectivity. I conducted this experiment using *Pseudomonas syringae* bacteria growing in Metapopulation Microcosm Plates (MMPs) with 96 wells, 95 of which were connected by 176 corridors. One unconnected well served as an uninoculated control for cross-contamination. All MMPs were produced and assembled as described in chapter 1. In each run of the experiment, parent plates of each corridor arrangement were needle inoculated in every well with *Pseudomonas syringae* pv. *syringae* B728a expressing gfp from an overnight culture at a concentration of 1.0-1.7 x 10^6 CFU/mL. The needles used for all inoculations in this experiment transferred 0.651 ± 0.347 (SD) µL volume, meaning that each well of the parent plates began with approximately 2.2-12.1 x 10^3 CFU/mL in each well. Parent plates were incubated at 22°C for 48 hours, and then subsampled into daughter plates with identical corridor arrangements using a plate replicator modified to produce the appropriate extinction pattern, as described below. Each daughter plate was incubated at 22°C for 156 hours and its fluorescence was measured in a microplate reader every 12 hours. All uninoculated controls remained sterile.

The three corridor arrangements were homogeneous, heterogeneous, and variable (Figure 2.1). In the homogeneous arrangement, wells were connected in an even lattice by 4.0 mm corridors. In the heterogeneous arrangement, wells were connected by corridors of variable lengths and well connectivities followed a right-skewed distribution such that a few wells were highly connected whereas most were directly connected to only one or two other wells. In the variable arrangement, the wells were connected in the even lattice arrangement of the homogeneous treatment but with corridor lengths that matched the heterogeneous treatment.

The extinction levels were 10% (10 wells) extinct, 50% (48 wells) extinct, 90% (86 wells) extinct, and a 0% no extinction control. Wells chosen for extinction in the daughter plates were driven extinct by removing their pins from the plate replicator (e.g. to create the 10% treatment, 10 pins were removed from the plate replicator). The identities of the extinct wells were chosen by sorting the wells of the heterogeneous corridor arrangement by their degree (number of neighbors; Figure 3.1). In the low connectivity extinction treatment, wells with the lowest degree were chosen for extinction. In the high connectivity extinction treatment, wells with the highest degree were chosen. When multiple wells had the same degree, they were chosen at random. The same well identities were extinguished in every corridor arrangement treatment, such that if well B6 was chosen as a high degree 10% extinction-level well, it was

made to go extinct in all high-connectivity 10% extinction-level plates. The full experiment was run three times, so that there were three plates of each treatment combination (n=3).

Statistical Methods

As a measure of well recovery following extinction, I calculated the deviation of each well on each treatment plate from the corresponding well on its control plate (the 0% extinction plate subsampled from the same parent plate), normalized to the control value and starting inoculum concentration, using the following formula:

$$Deviation\ from\ Control = ((Fluor_T/Start)-(Fluor_C/Start))/(Fluor_C/Start),$$

where $Fluor_T$ is the fluorescence of the treatment well, $Fluor_C$ is the fluorescence of the corresponding control well, and *Start* is the concentration of the culture from which the parent plate was inoculated (Figures 2.4 and 2.5). I used this quantity to calculate three recovery metrics:

1) Time to Begin Recovery Phase – I defined the recovery phase of each plate's time series as the portion during which the change in deviation from the control was positive (i.e. the treatment plate was becoming more similar to the control). I calculated the time at which this recovery phase began for each plate.

2) Maximum Rate of Recovery – I fit each recovery phase with linear, quadratic, cubic, and quartic regressions and chose the model that best fit the data using AICc model selection. I then found the derivative of each best-fit model and used it to calculate the maximum rate of recovery during the recovery phase for each treatment.

3) Time to Recovery – Using a planned contrast at each time step, I defined the time to recovery as the first time period during which there was no significant difference between the treatment and control.

I calculated all three metapopulation level metrics for each combination of corridor arrangement, extinction level, and extinction connectivity on two datasets: one including the mean of all subpopulations in each plate and one including the plate mean of only those subpopulations targeted for extinction. To assess whether variability in re-colonization affected the recovery of the metapopulations, I also calculated the standard deviation of Deviation from Control of the wells of each plate.

Finally, focusing on the subpopulations, I fit several multiple polynomial regression models using each well's Deviation from Control as the response variable. Hours post-extinction, hours post-extinction squared, and hours post-extinction cubed were included as explanatory variables in all models. One or more of the following were also included in each model as explanatory variables: corridor arrangement, extinction level, the interaction between corridor arrangement and extinction level, extinction connectivity (low or high treatment), well connectivity (number of corridors by which each well is connected to the network), and interior-or-exterior (a categorical variable describing whether the well was on the interior or edge of the plate). I chose the model with the lowest AIC_c value as the best-fit model. I performed this

procedure on two datasets, one including all subpopulations and one comprised only of subpopulations targeted for extinction. I assessed homogeneity of variance and normality of residuals by plotting the residuals. All analyses were performed in R (R Core Team, 2016), with models fit using the nmle package (Pinheiro, Bates, DebRoy, Sarkar, & {R Core Team}, 2017) and the planned contrast performed in multcomp (Hothorn, Bretz, & Westfall, 2008). Figures were produced using the ggplot2 package (Wickham, 2009).

In all runs of this experiment, MMPs were filled with Luria-Bertani liquid medium (LB; Cold Spring Harbor Protocols, 2006) containing 40 µg/mL nitrofurantoin and 15 µg/mL tetracycline to select against loss of mutant plasmids. This experiment was performed using wild type *Pseudomonas syringae* pv. *syringae* B728a containing the *pkln42gfp* plasmid, which constitutively expresses *gfp* (Dulla & Lindow, 2008). This strain is motile and doubles approximately every 3 h at 15℃ in this set-up. This *Pseudomonas* strain was generously provided to me by the Lindow Lab, UC Berkeley.

Results

Time to Begin Recovery Phase

All 50% extinction metapopulations began to recover (approach their controls) after 24 hours. All 90% extinction metapopulations began to recover after 36 hours. In contrast, the recovery behavior of the 10% extinction metapopulations was variable and depended on their corridor heterogeneity and the connectedness (degree) of their extinct wells (Table 3.1a). Recovery of metapopulations with heterogeneous corridors differed depending on whether extinct wells had low or high degree. Heterogeneous metapopulations in which low-degree wells were targeted for extinction began to recover after 36 hours, whereas recovery began after 24 hours when high-degree wells were targeted for extinction. Metapopulations with variable corridors began to recover after 24 hours and homogeneous metapopulations began to recover after 12 hours, regardless of whether extinctions targeted high or low-degree wells. When considering recovery of individual subpopulations targeted for extinction, all extinct subpopulations in the 10% and 50% extinction metapopulations began to recover after 24 hours and all extinct subpopulations in the 90% extinction metapopulations began to recover after 36 hours (Table 3.1b).

Final Mean Size of Subpopulations

In general, the metapopulations experiencing 10% extinction recovered to the highest maximum mean subpopulation sizes (relative to their controls), 50% extinction recovered to intermediate subpopulation sizes, and the 90% extinction treatment reached the lowest subpopulations sizes. Within this general pattern, however, corridor arrangement of the metapopulation and degree of the subpopulations targeted for extinction affected the average final size reached by recovering subpopulations (Figure 3.2a).

In the 10% extinction treatment, metapopulations with homogeneous corridors reached higher subpopulation sizes than those with heterogeneous corridors, and within each corridor arrangement, subpopulations reached the highest average size when high-degree subpopulations were targeted for extinction. Among metapopulations with variable corridors, the 10% extinction

treatment caused radically different effects depending on whether high-degree or low-degree subpopulations were targeted for extinction, such that subpopulations reached the lowest average size when low-degree subpopulations were targeted for extinction and the highest average size when high-degree subpopulations were targeted for extinction.

In the 50% extinction treatment, subpopulations recovered to higher sizes when high-degree subpopulations were targeted for extinction, but recovery varied with corridor arrangement. Under this extinction treatment, subpopulation recovery size was highest in the homogeneous corridor arrangement, intermediate in the heterogeneous corridor arrangement, and lowest in the variable corridor arrangement. In contrast, when low-degree subpopulations were targeted for extinction, subpopulation recovery size was highest in the heterogeneous corridor arrangement, intermediate in the variable corridor arrangement, and lowest in the homogeneous corridor arrangement.

In contrast to the 50% extinction treatment, in the 90% extinction treatment subpopulations reached the highest sizes when low-degree populations were targeted for extinction. Again, recovery varied with corridor arrangement. Under this extinction treatment, subpopulations reached the highest sizes in metapopulations with a variable corridor arrangement, intermediate sizes in the heterogeneous arrangement, and lowest sized in the homogeneous arrangement. This pattern shifted when high-degree subpopulations were targeted for extinction, such that subpopulations reached the highest size in metapopulations with homogeneous corridor arrangements, intermediate size in those with variable corridors, and the lowest size in those with heterogeneous corridors.

Recovery size patterns of wells targeted for extinction, were similar except for the following. First, in the 10% extinction treatment, subpopulation sizes reached by the heterogeneous metapopulations with high-degree wells targeted for extinction exceeded that of the homogeneous metapopulations with low-degree wells targeted for extinction. Also in the 10% extinction treatment, when low-degree wells were targeted for extinction, subpopulation sizes in variable metapopulations were higher than those in heterogeneous metapopulations. Finally, in the 50% extinction treatment, when low-degree wells were targeted for extinction, the subpopulation sizes of homogeneous metapopulations exceeded those of variable metapopulations (Figure 3.2b).

Standard Deviation of Deviation from Control

Standard deviation of the “Deviation from Control” response variable was highest in the 90% extinction treatment, intermediate in the 50% extinction treatment, and lowest in the 10% extinction treatment (Figure 3.3a). Within this general pattern, as described below, corridor arrangement of the metapopulation and degree of the subpopulations targeted for extinction affected the average size reached by recovering subpopulations.

Within the 10% extinction treatment, the standard deviation was highest when extinction targeted low-degree subpopulations in heterogeneous and variable corridor metapopulations, intermediate when extinction targeted high-degree subpopulations in homogeneous and heterogeneous metapopulations, and lowest either when extinction targeted high-degree subpopulations in homogeneous metapopulations or low-degree subpopulations in variable metapopulations. Within the 50% and 90% extinction treatments, the standard deviation was highest in heterogeneous metapopulations, intermediate in variable metapopulations, and lowest in homogeneous metapopulations, but was influenced by which wells were targeted for

extinction. In the 50% extinction treatment of heterogeneous metapopulations, standard deviation was highest when low-degree wells were targeted, was not affected by well-degree in variable metapopulations, and was highest when high-degree wells were targeted in homogeneous metapopulations. In the 90% extinction treatment, within each corridor arrangement, standard deviation was highest when high-degree wells were targeted for extinction.

The patterns were generally the same amongst extinct wells, except in the 10% extinction treatment where the high connectivity variable and low connectivity heterogeneous had the highest standard deviation, intermediate in low connectivity variable and high connectivity heterogeneous, and lowest in low and high connectivity homogeneous. And, in the 50% extinction treatment, the standard deviations of low and high connectivity homogeneous metapopulations were very similar (Figure 3.3b).

Maximum Rate of Recovery

Using the dataset including all subpopulations, the mean recoveries of most metapopulations were fit best by cubic models for most treatment combinations (Table 3.2). However, quadratic models best fit the 10% extinction targeting low-degree subpopulations, the 90% extinction targeting high-degree subpopulations in heterogeneous corridors, the 50% extinction targeting high-degree subpopulations in homogeneous corridors, and the 10% extinction targeting low-degree subpopulations in variable corridors. Linear models provided the best fit for treatments with homogeneous corridors and either 10% extinction or 50% extinction targeting low-degree subpopulations, and 10% extinction targeting high-degree subpopulations in variable corridors (Table 3.2).

The recoveries of extinct subpopulations were fit best by cubic models for most treatment combinations (Table 3.3). However, quadratic models best fit the 10% and 90% extinctions in which high-degree wells were targeted in heterogeneous corridor arrangements, 10% and 50% extinctions in which high-degree wells were targeted in homogeneous arrangements, and in variable arrays in which either 10% extinction targeted high-degree wells or 50% extinction targeted low-degree wells. Finally, a quartic model provided the best fit when 50% extinction targeted high-degree wells in metapopulations with heterogeneous corridors.

Given the model choices described above, when considering the mean recovery of all subpopulations, the maximum rate of recovery for most combinations of extinction level and well-degree was highest in metapopulations with heterogeneous corridor arrangements, lowest in those with homogeneous arrangements, and intermediate in those with variable arrangements (Figure 3.4a). However, when 90% extinction targeted high-degree wells, the recovery rate of metapopulations with variable corridors exceeded those with heterogeneous corridors. Among metapopulations with heterogeneous corridors, the highest maximum rate of recovery occurred when 50% extinction targeted low-degree wells, whereas the maximum rates of recovery for metapopulations with homogeneous and variable corridor arrangements occurred when 90% extinction targeted the low-degree wells.

When the same analysis was applied to the dataset including only subpopulations targeted for extinction, the patterns were similar, except that the maximum rate of recovery for metapopulations with the variable corridor arrangement was intermediate to that of the heterogeneous and homogeneous arrangements in the 90% extinction that targeted low-degree

wells , but exceeded both corridor arrangements in the 50% extinction that targeted high-degree wells (Figure 3.4b).

Time to Recovery

When considering the dataset with all subpopulations, the time for an extinction-treated metapopulation to become statistically indistinguishable from its control differed with its extinction treatment and corridor arrangement (Figure 3.5a). In the 10% extinction in which low-degree wells were targeted, metapopulations with a heterogeneous corridor arrangement recovered after 60 hours, whereas homogeneous and variable metapopulations took only 48 hours. When 10% extinction targeted high-degree wells, heterogeneous metapopulations took 36 hours to recover and variable metapopulations took 24 hours, whereas homogeneous metapopulations never recovered to the control condition. In the 50% extinction in which low-degree wells were targeted, heterogeneous metapopulations took 72 hours to recover whereas variable and homogeneous metapopulations never recovered. In contrast, when 50% extinction targeted high-degree wells, heterogeneous and variable metapopulations took 48 hours to recover and homogeneous metapopulations took 36 hours. No metapopulations recovered to the control condition following a 90% extinction treatment.

When considering the dataset including only subpopulations targeted for extinction (Figure 3.5b), with a 10% extinction targeting low-degree wells, extinct subpopulations took an average of 108 hours to recover in heterogeneous metapopulations, 72 hours in variable metapopulations, and 60 hours in homogeneous metapopulations. In the 10% extinction targeting high-degree wells, heterogeneous metapopulations took 60 hours to recover, and homogeneous and variable metapopulations took 12 hours to recover. In the 50% extinction targeting low-degree wells, heterogeneous metapopulations took 84 hours to recover. In the 50% extinction targeting high-degree wells, all corridor arrangements recovered after 72 hours.

Polynomial Regression

The polynomial regression model of all subpopulation recoveries containing all terms except well connectivity fit the data better than all other models (Table 3.4). For the dataset containing only extinct subpopulations, the full polynomial regression, which contained all terms including well connectivity, fit the data better than all other models (Table 3.5).

Discussion

In three respects, the results of this experiment matched those of a previous experiment in which extinction targeted random subpopulations (i.e. without considering their connectivity, as in Chapter 2). First, in both experiments, metapopulations with heterogeneous corridor arrangements had the fastest rate of recovery from almost all combinations of extinction level and extinction connectivity. However, following low-level extinction (10% of subpopulations), metapopulations with heterogeneous corridors took longer to recover than those with homogeneous or variable corridors, regardless of whether extinctions targeted high- or low-

connectivity subpopulations. Third, in neither experiment did any metapopulations recover from the highest level of extinction (90% of subpopulations), regardless of its pattern.

In several ways, however, results of the moderate level of extinction (50% of subpopulations) differed between this experiment and the random-extinction experiment. For example, when extinction occurred randomly, recovery from moderate-level extinction took longer for metapopulations with homogeneous corridors than for those with heterogeneous corridors (Chapter 2). However, when extinctions targeted highly connected subpopulations, recovery from moderate-level extinction took slightly less time for metapopulations with homogeneous corridors than for those with either heterogeneous or variable corridors, each of which recovered over the same amount of time. Finally, when moderate-level extinctions targeted low-connectivity subpopulations, homogeneous and variable metapopulations were unable to recover at all during the experiment.

Addressing the last point first, one reason a metapopulation might fail to recover from a particular level or pattern of extinction is that it simply needed more time than was available during an experiment of pre-determined length. By this logic, one could infer that recovery from moderate-level extinction targeted at poorly connected subpopulations takes longer for metapopulations with homogeneous or variable corridor arrangements than for those with heterogeneous corridor arrangements. In contrast to this interpretation, however, recovery from moderate-level extinction targeted at poorly connected subpopulations actually followed a pattern similar to that observed when extinction randomly targets subpopulations. That is, metapopulations with heterogeneous corridors recovered faster than those with homogeneous corridors. However, the pattern differed when extinction targeted highly-connected subpopulations.

As with recovery following random extinctions (Chapter 2), in this experiment, no metapopulations recovered from high-level (90%) extinction. However, the maximum rates of recovery of the three corridor arrangements were much closer to each other following high-level extinction than following any other extinction level. Further, within each extinction connectivity treatment at this extinction level, metapopulations with heterogeneous corridors deviated much farther from their controls than did those with homogeneous corridors, suggesting that those with heterogeneous corridors ultimately would have recovered more slowly.

How well do these patterns support my predictions? First, I had predicted that metapopulations with heterogeneous corridors would recover faster from extinctions targeting poorly connected subpopulations than those targeting highly connected subpopulations. The data did not consistently support that prediction. Instead, when recovering from high-level extinction, the type of subpopulation targeted for extinction affected the recovery rate of metapopulations with heterogeneous corridors differently depending on the severity of extinction. My prediction was supported at the highest extinction level, but the other extinction levels did not support my prediction. At the intermediate extinction level, the recovery rate of heterogeneous metapopulations was not affected by whether extinction targeted highly or poorly connected subpopulations. And, at the lowest extinction level, these heterogeneous metapopulations recovered faster from extinction that targeted highly connected subpopulations than when it targeted poorly connected subpopulations.

I had also predicted that the degree of connectivity of subpopulations targeted for extinction treatment would not affect the recovery of metapopulations with homogeneous corridor arrangements. However, extinct subpopulations in homogeneous metapopulations displayed the same pattern as those in heterogeneous metapopulations, albeit to a lesser degree,

with slightly slower rates of recovery when extinctions were in high connectivity subpopulations than when they were in low connectivity subpopulations. Again, faster recovery rates of subpopulations targeted for extinction only translated into a faster rate of metapopulation recovery when low connectivity subpopulations were targeted for the highest extinction level. At the moderate extinction level, recovery was slightly faster following high connectivity extinctions, and in the 10% extinction level treatment, rates of recovery were similar between the two extinction connectivity treatments.

Why did metapopulations with homogeneous corridors respond to extinction in patterns similar to those exhibited by metapopulations with heterogeneous corridors? There are two possible explanations for this deviation from model predictions. First, models assume ideal homogeneous metapopulations, in which every node has the same degree, but, as with any real metapopulation, the metapopulations created in the MMPs have edges, which reduces the connectivities of edge and corner subpopulations. While every well in the interior of my experimental metapopulations was connected to four neighbors, wells on the straight edges were connected to only three and those at the corners, to only two neighbors. The second possible explanation is that evaporative edge effects changed the behavior of edge wells, which were also physically at the edge of the MMPs. Unfortunately, both mechanisms could have affected the same wells in the MMPs, which might make them difficult to disentangle statistically. However, evaporative edge effects would reduce the volume of medium, causing the same number of bacteria to be denser, which would artificially inflate subpopulation size. Thus, in homogeneous metapopulations, excess evaporation at the edges would cause subpopulations with low connectivity to consistently have the highest subpopulation sizes. However, plotting the change in Deviation from the Control over time in subpopulations with different connectivities demonstrates that the difference in recovery of metapopulations with homogeneous corridors following extinctions in low versus high connectivity wells cannot be attributed to edge effects alone. Instead, as expected from network heterogeneity, on average the low connectivity wells had the highest subpopulation sizes only when extinction targeted high connectivity wells and the lowest sizes when extinction targeted low connectivity wells. Thus, the variation in connectivity found in edge and corner wells does appear to reduce the degree homogeneity of nodes in the homogeneous metapopulation treatment. In turn, this heterogeneity causes the degree of connectivity of subpopulations targeted for extinction to affect the recovery of these metapopulations, albeit less than was observed with the metapopulations with deliberately heterogeneous corridor arrangements. These results thus support the hypothesis that the connectivity of the subpopulations that go extinct affects the rate of recovery of heterogeneous metapopulations. Moreover, because the pattern was weaker for the homogeneous metapopulation treatment, the result suggests that the degree of heterogeneity influences the magnitude of this effect.

As anthropogenic habitat fragmentation becomes more widespread and human-made dispersal corridors are increasingly used to provide pathways for organisms between otherwise isolated patches, it is important to understand how the placement of those corridors on the landscape may affect the populations they are designed to assist. The results of this experiment suggest that spatial clustering of dispersal corridors in metapopulations may help to alleviate the effects of habitat fragmentation in some circumstances, but exacerbate them in others. While a homogeneous corridor arrangement may be beneficial when subpopulation extinction levels are relatively low, at high extinction rates a heterogeneous arrangement may better facilitate recovery. And when extinctions differentially affect high versus low

connectivity subpopulations, the importance of corridor arrangement for recovery may depend on the extinction rate of subpopulations. These results demonstrate that while taking a network-theoretic approach to metapopulation ecology may facilitate the use of research on other types of networks to make useful predictions, other comparisons will likely be less fruitful. Only by testing these predictions experimentally can we understand how the spatial arrangement of dispersal corridors affects metapopulation dynamics.

Table 3.1. Hours to beginning of recovery phase for each combination of corridor arrangement by extinction level by extinction connectivity treatment for a) all wells and b) extinct wells only (no variation between replicates).

a)

Corridor Arrangement	Extinction Level					
	10%		50%		90%	
Extinction Connectivity	Low	High	Low	High	Low	High
Heterogeneous	36	24	24	24	36	36
Homogeneous	12	12	24	24	36	36
Variable	24	24	24	24	36	36

b)

Corridor Arrangement	Extinction Level					
	10%		50%		90%	
Extinction Connectivity	Low	High	Low	High	Low	High
Heterogeneous	24	24	24	24	36	36
Homogeneous	24	24	24	24	36	36
Variable	24	24	24	24	36	36

Table 3.2. Akaike's Information Criterion (corrected) for linear, quadratic, cubic, and quartic fits of deviation from control (response variable) to hours post-extinction (explanatory variable) for each corridor arrangement by extinction level treatment combination for all wells. Asterisks indicate lowest AIC_c value for each treatment combination.

Corridor Arrangement	Extinction Connectivity	Extinction Level: 10% Low	10% High	50% Low	50% High	90% Low	90% High
Heterogeneous	Linear	-40.49	-31.55	-19.86	-23.94	-20.87	-28.97
	Quadratic	-48.68 *	-41.03	-41.36	-35.86	-42.06	-41.85 *
	Cubic	-47.97	-51.69 *	-61.77 *	-53.44 *	-61.48 *	-40.50
	Quartic	-40.57	-43.14	-57.19	-44.69	-55.73	-35.93
Homogeneous	Linear	-50.72 *	-37.48 *	-52.63 *	-35.53	-36.29	-42.49
	Quadratic	-46.42	-37.25	-52.56	-38.82 *	-54.81	-61.27
	Cubic	-40.88	-34.54	-49.05	-34.41	-57.27 *	-64.07 *
	Quartic	-34.72	-34.51	-40.34	-30.43	-46.73	-54.13
Variable	Linear	-66.53	-58.98 *	-28.00	-33.39	-25.53	-34.84
	Quadratic	-67.73 *	-58.05	-49.89	-40.01	-38.48	-47.98
	Cubic	-61.76	-52.40	-74.56 *	-43.60 *	-46.10 *	-51.87 *
	Quartic	-60.35	-45.65	-65.80	-38.09	-35.91	-41.02

Table 3.3. Akaike's Information Criterion (corrected) for linear, quadratic, cubic, and quartic fits of Deviation from Control (response variable) to the explanatory variable, hours post-extinction, for each combination of corridor arrangement by extinction level for a) all wells and b) only wells targeted for extinction. Asterisks indicate lowest AIC_c value for each treatment combination.

			Extinction Level					
			10%		50%		90%	
Corridor Arrangement		Extinction Connectivity	Low	High	Low	High	Low	High
	Heterogeneous	Linear	-24.62	-19.63	-16.88	-16.63	-18.41	-27.18
		Quadratic	-39.75	-30.53 *	-40.67	-32.92	-39.13	-41.68 *
		Cubic	-41.01 *	-27.19	-43.72 *	-32.29	-59.09 *	-40.89
		Quartic	-33.52	-24.87	-36.72	-35.13 *	-55.01	-37.03
	Homogeneous	Linear	-44.11	-31.75	-38.28	-33.70	-32.02	-39.17
		Quadratic	-54.86	-34.94 *	-50.42	-42.63 *	-49.11	-57.85
		Cubic	-59.02 *	-30.78	-54.28 *	-37.90	-56.08 *	-63.49 *
		Quartic	-50.26	-25.68	-48.92	-31.50	-47.45	-53.24
	Variable	Linear	-30.31	-40.65	-24.74	-27.21	-23.69	-34.321
		Quadratic	-53.72	-45.66 *	-42.08 *	-45.01	-37.70	-48.80
		Cubic	-58.25 *	-41.09	-37.39	-50.14 *	-45.23 *	-49.94 *
		Quartic	-50.84	-35.36	-32.26	-41.51	-35.02	-38.94

Table 3.4. Akaike's Information Criterion (corrected) for multiple polynomial regression fits of deviation from control (response variable), linear, squared, and cubic terms for hours post-extinction (HPE), and corridor arrangement (Corr), extinction level (Ext), the interaction between corridor arrangement and extinction level (Corr:Ext), low/high extinction connectivity (Low), connectivity (Conn), and interior/edge position (Edge) for all subpopulations. Asterisks indicate best-fit models.

Model (Right-hand side)	AIC_c
HPE + HPE^2 + HPE^3 + Corr + Ext + Corr:Ext + Low + Conn + Edge	-2106.61
HPE + HPE^2 + HPE^3 + Corr + Ext + Corr:Ext + Low + Conn	-2026.72
HPE + HPE^2 + HPE^3 + Corr + Ext + Corr:Ext + Low + Edge	-2108.38 *
HPE + HPE^2 + HPE^3 + Corr + Ext + Corr:Ext + Conn + Edge	-2096.56
HPE + HPE^2 + HPE^3 + Corr + Low + Conn + Edge	21214.72
HPE + HPE^2 + HPE^3 + Ext + Low + Conn + Edge	-1432.57
HPE + HPE^2 + HPE^3 + Corr + Ext + Corr:Ext + Low	-2004.43
HPE + HPE^2 + HPE^3 + Corr + Ext + Corr:Ext + Conn	-2016.69
HPE + HPE^2 + HPE^3 + Corr + Low + Conn	21266.89
HPE + HPE^2 + HPE^3 + Ext + Low + Conn	-1353.05
HPE + HPE^2 + HPE^3 + Corr + Ext + Corr:Ext + Edge	-2098.33
HPE + HPE^2 + HPE^3 + Corr + Low + Edge	21212.87
HPE + HPE^2 + HPE^3 + Ext + Low + Edge	-1434.28
HPE + HPE^2 + HPE^3 + Corr + Conn + Edge	21220.57
HPE + HPE^2 + HPE^3 + Ext + Conn + Edge	-1422.67
HPE + HPE^2 + HPE^3 + Low + Conn + Edge	21399.28
HPE + HPE^2 + HPE^3 + Corr + Ext + Corr:Ext	-1994.40
HPE + HPE^2 + HPE^3 + Corr + Low	21280.97
HPE + HPE^2 + HPE^3 + Corr + Conn	21272.73
HPE + HPE^2 + HPE^3 + Corr + Edge	21218.72
HPE + HPE^2 + HPE^3 + Ext + Low	-1331.60
HPE + HPE^2 + HPE^3 + Ext + Conn	-1343.16
HPE + HPE^2 + HPE^3 + Ext + Edge	-1424.37
HPE + HPE^2 + HPE^3 + Low + Conn	21451.69
HPE + HPE^2 + HPE^3 + Low + Edge	21397.48
HPE + HPE^2 + HPE^3 + Conn + Edge	21405.10
HPE + HPE^2 + HPE^3 + Corr	21286.80
HPE + HPE^2 + HPE^3 + Ext	-1321.72
HPE + HPE^2 + HPE^3 + Low	21465.34
HPE + HPE^2 + HPE^3 + Conn	21457.50
HPE + HPE^2 + HPE^3 + Edge	21403.30
HPE + HPE^2 + HPE^3	21471.15

Table 3.5. Akaike's Information Criterion (corrected) for multiple polynomial regression fits of deviation from control (response variable), linear, squared, and cubic terms for hours post-extinction (HPE), and corridor arrangement (Corr), extinction level (Ext), the interaction between corridor arrangement and extinction level (Corr:Ext), low/high extinction connectivity (Low), connectivity (Conn), and interior/edge position (Edge) for extinct subpopulations only. Asterisks indicate best-fit models.

Model (Right-hand side)	AIC_c
HPE + HPE^2 + HPE^3 + Corr + Ext + Corr:Ext + Low + Conn + Edge	2705.01 *
HPE + HPE^2 + HPE^3 + Corr + Ext + Corr:Ext + Low + Conn	3091.56
HPE + HPE^2 + HPE^3 + Corr + Ext + Corr:Ext + Low + Edge	2838.22
HPE + HPE^2 + HPE^3 + Corr + Ext + Corr:Ext + Conn + Edge	2921.01
HPE + HPE^2 + HPE^3 + Corr + Low + Conn + Edge	9998.90
HPE + HPE^2 + HPE^3 + Ext + Low + Conn + Edge	2991.34
HPE + HPE^2 + HPE^3 + Corr + Ext + Corr:Ext + Low	3658.15
HPE + HPE^2 + HPE^3 + Corr + Ext + Corr:Ext + Conn	3268.99
HPE + HPE^2 + HPE^3 + Corr + Low + Conn	10198.74
HPE + HPE^2 + HPE^3 + Ext + Low + Conn	3398.36
HPE + HPE^2 + HPE^3 + Corr + Ext + Corr:Ext + Edge	3014.00
HPE + HPE^2 + HPE^3 + Corr + Low + Edge	10196.77
HPE + HPE^2 + HPE^3 + Ext + Low + Edge	3098.32
HPE + HPE^2 + HPE^3 + Corr + Conn + Edge	10172.63
HPE + HPE^2 + HPE^3 + Ext + Conn + Edge	3200.54
HPE + HPE^2 + HPE^3 + Low + Conn + Edge	10065.68
HPE + HPE^2 + HPE^3 + Corr + Ext + Corr:Ext	3737.48
HPE + HPE^2 + HPE^3 + Corr + Low	10750.52
HPE + HPE^2 + HPE^3 + Corr + Conn	10347.34
HPE + HPE^2 + HPE^3 + Corr + Edge	10326.61
HPE + HPE^2 + HPE^3 + Ext + Low	3910.55
HPE + HPE^2 + HPE^3 + Ext + Conn	3568.06
HPE + HPE^2 + HPE^3 + Ext + Edge	3272.44
HPE + HPE^2 + HPE^3 + Low + Conn	10265.85
HPE + HPE^2 + HPE^3 + Low + Edge	10261.36
HPE + HPE^2 + HPE^3 + Conn + Edge	10238.77
HPE + HPE^2 + HPE^3 + Corr	10812.13
HPE + HPE^2 + HPE^3 + Ext	3989.15
HPE + HPE^2 + HPE^3 + Low	10813.79
HPE + HPE^2 + HPE^3 + Conn	10413.83
HPE + HPE^2 + HPE^3 + Edge	10390.89
HPE + HPE^2 + HPE^3	10875.25

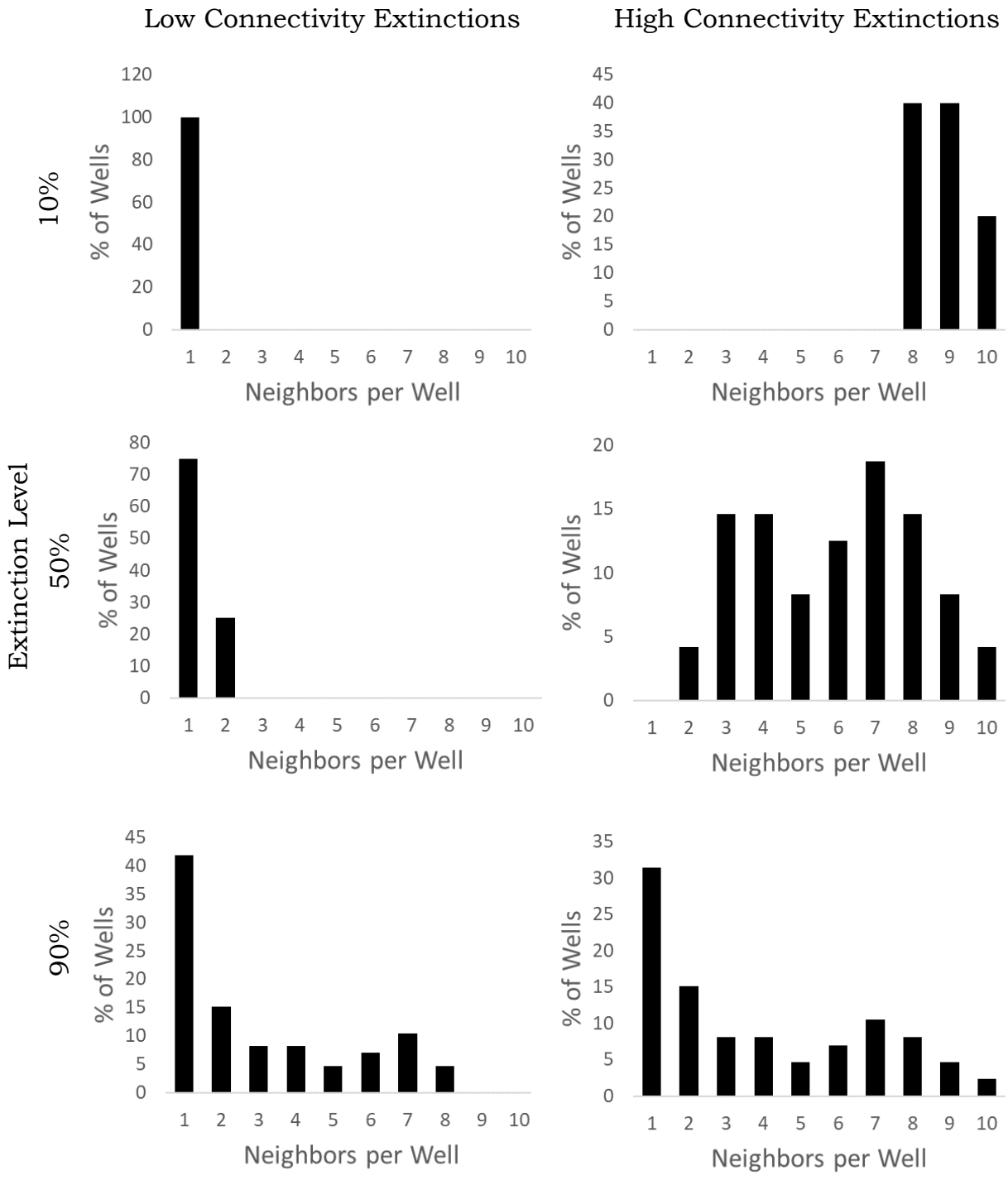

Figure 3.1. Neighbors per subpopulation for all extinct subpopulations in low connectivity extinction treatments (left) and high connectivity extinction treatments (right) and 10% extinction level treatments (top), 50% extinction level treatments (middle), and 90% extinction level treatments (bottom).

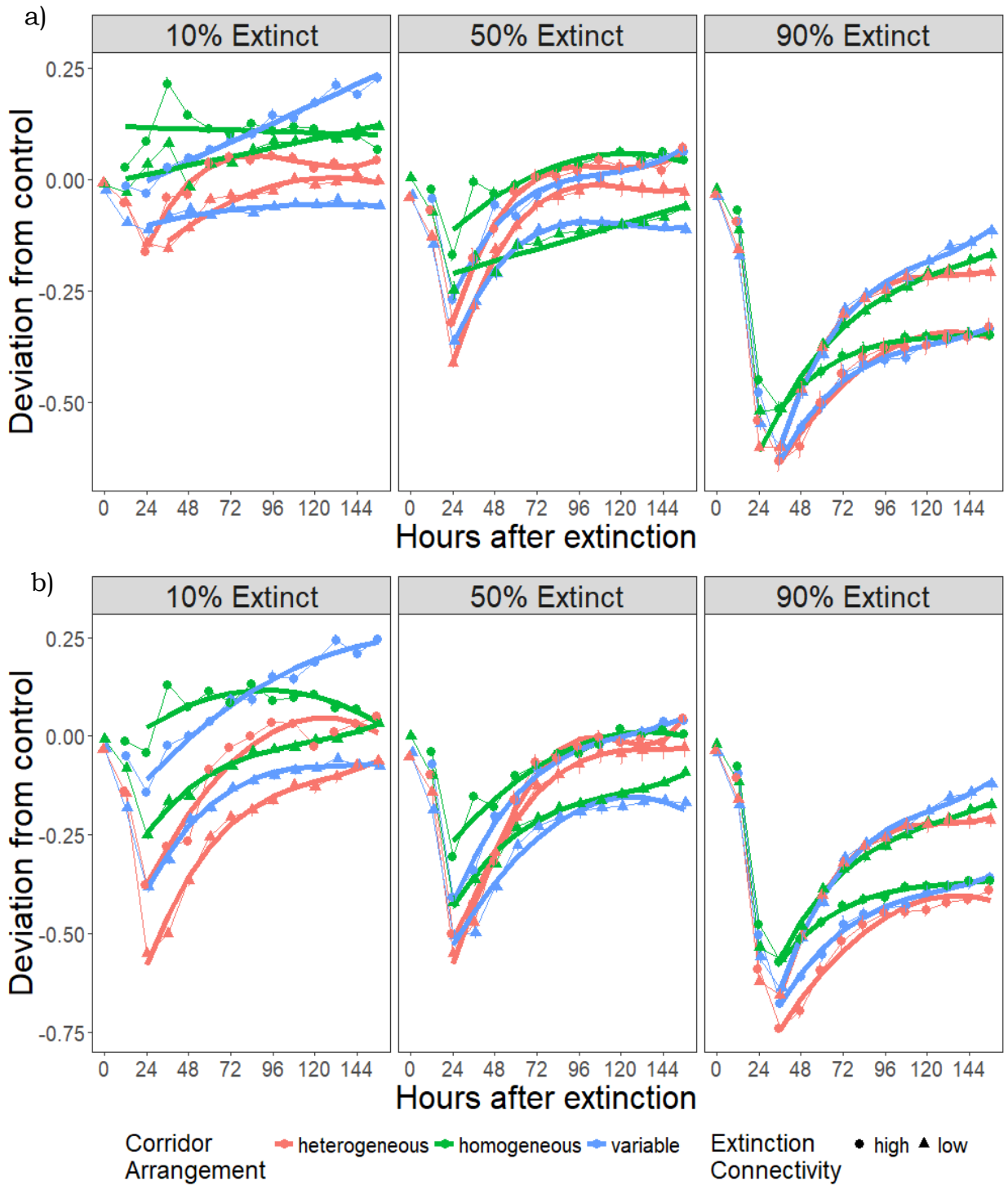

Figure 3.2. Deviation of treatment plates from control plates with heterogeneous, homogeneous, or variable corridor arrangements following 10%, 50%, or 90% extinction in low or high connectivity wells of a) all subpopulations or b) extinct subpopulations only. Error bars are standard error of the mean (n=3). Thick lines are best fit lines for each recovery trajectory.

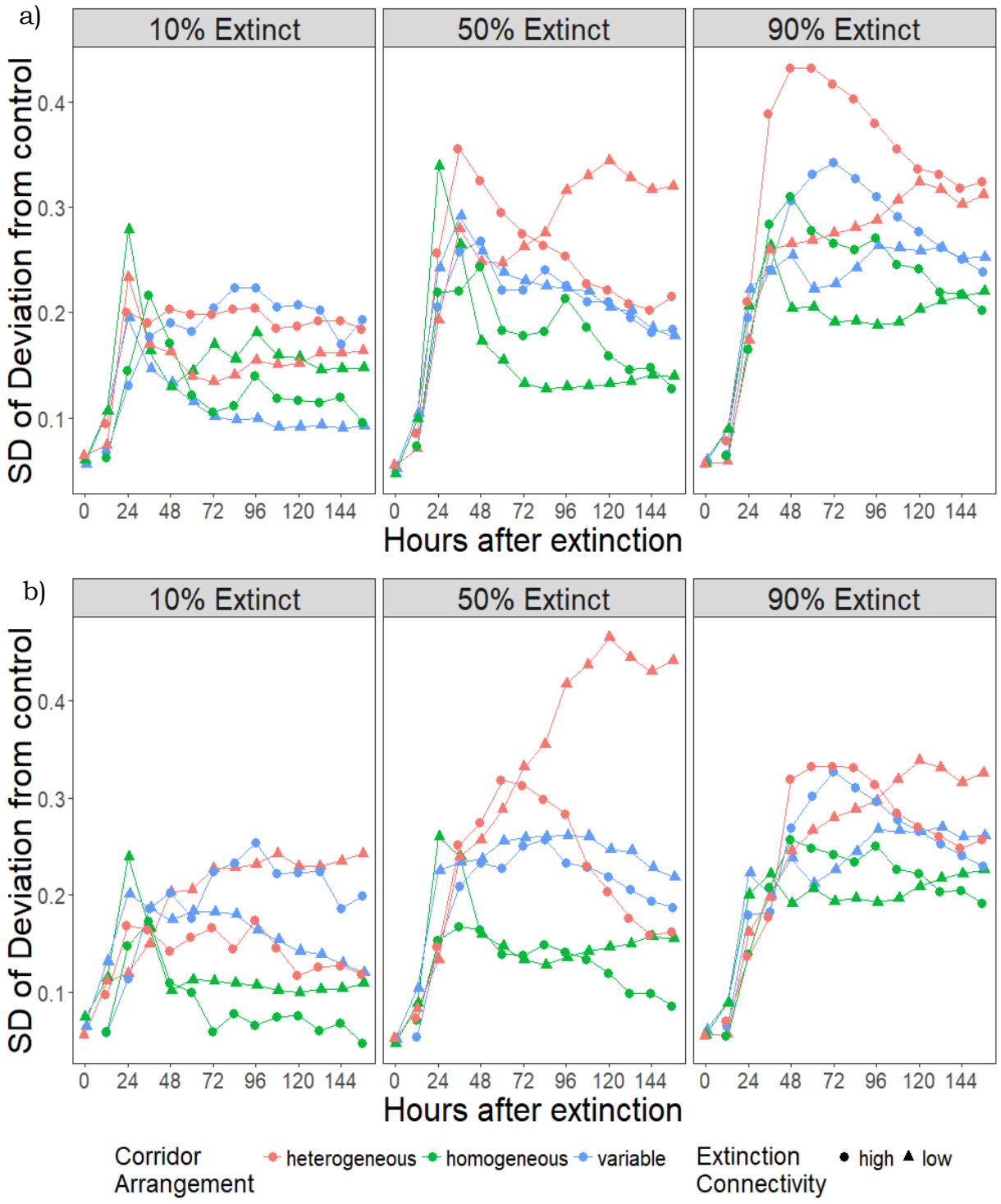

Figure 3.3. Standard deviation of "deviation from control" response variable for heterogeneous, homogeneous, or variable corridor arrangements following 10%, 50%, or 90% extinction in low or high connectivity wells of a) all subpopulations or b) extinct subpopulations only.

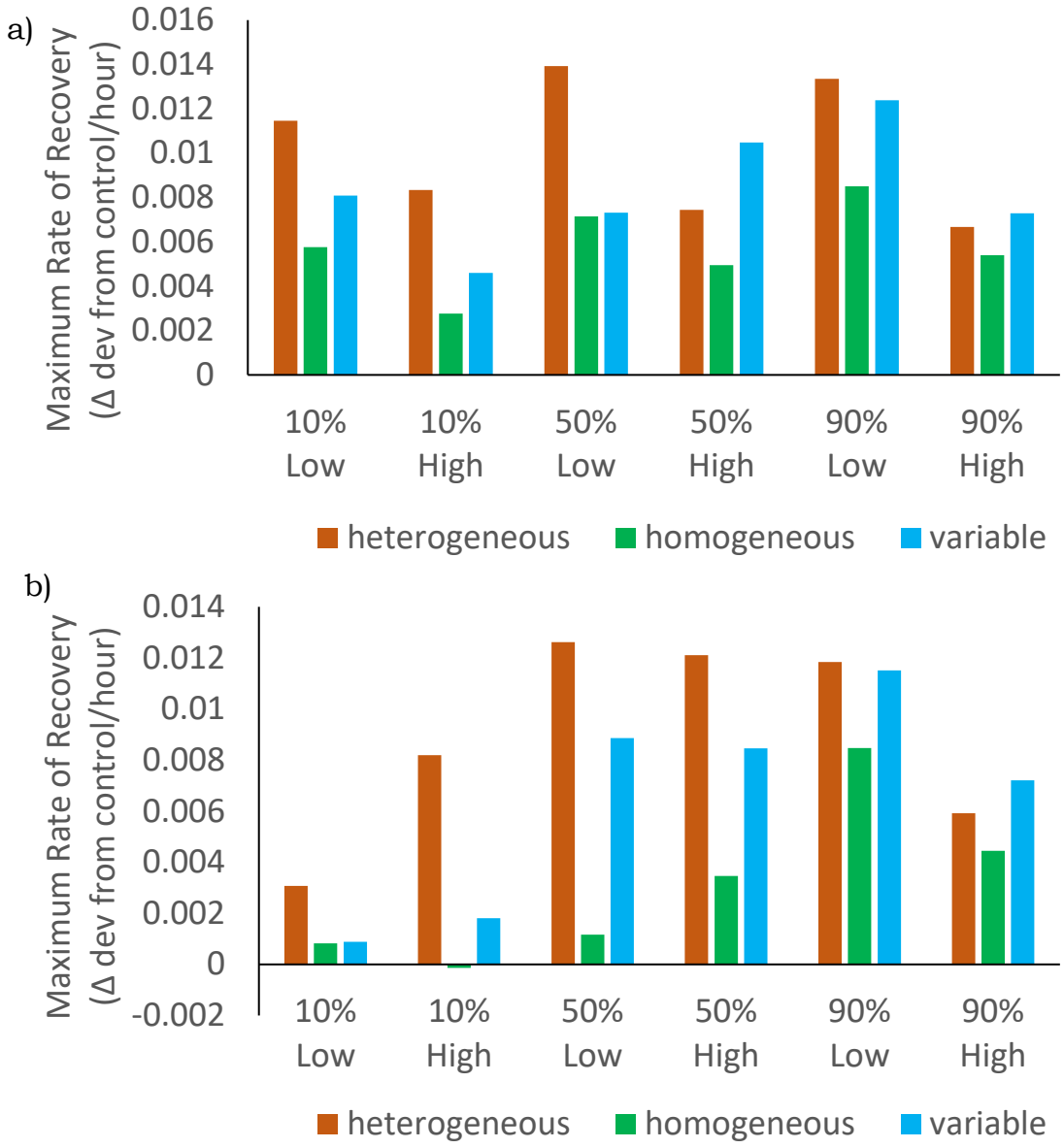

Figure 3.4. Maximum rate of recovery, measured as change in "deviation from control" response variable per hour, for each combination of corridor arrangement, extinction level, and extinction connectivity for a) all subpopulations and b) extinct subpopulations only. This recovery rate maximum was calculated by finding the maximum derivative of the best-fit model [see Tables 3.2 and 3.3] during the recovery phase.

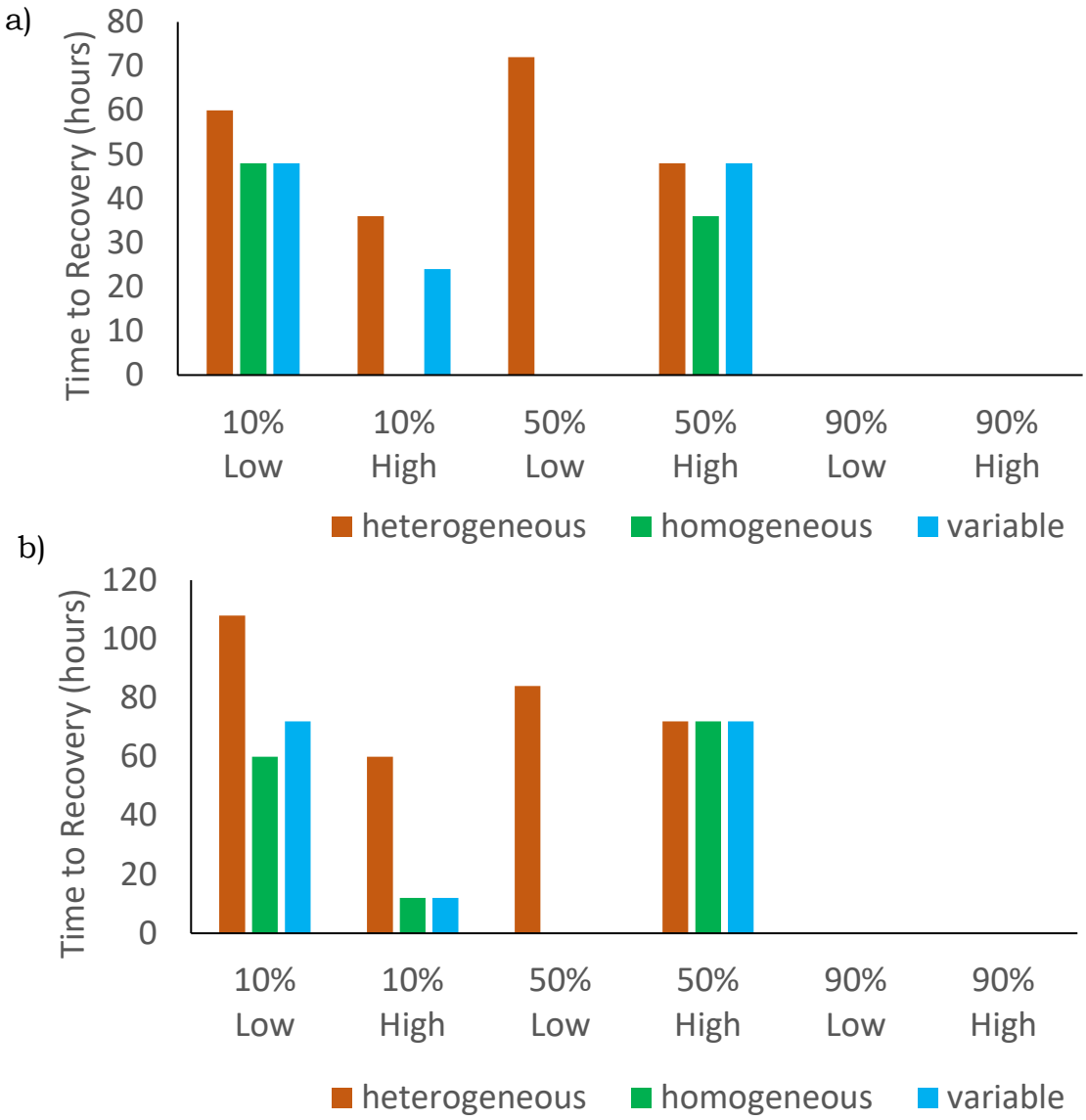

Figure 3.5. Hours to recovery for each combination of corridor arrangement, extinction level, and extinction connectivity for a) all subpopulations and b) extinct subpopulations only.

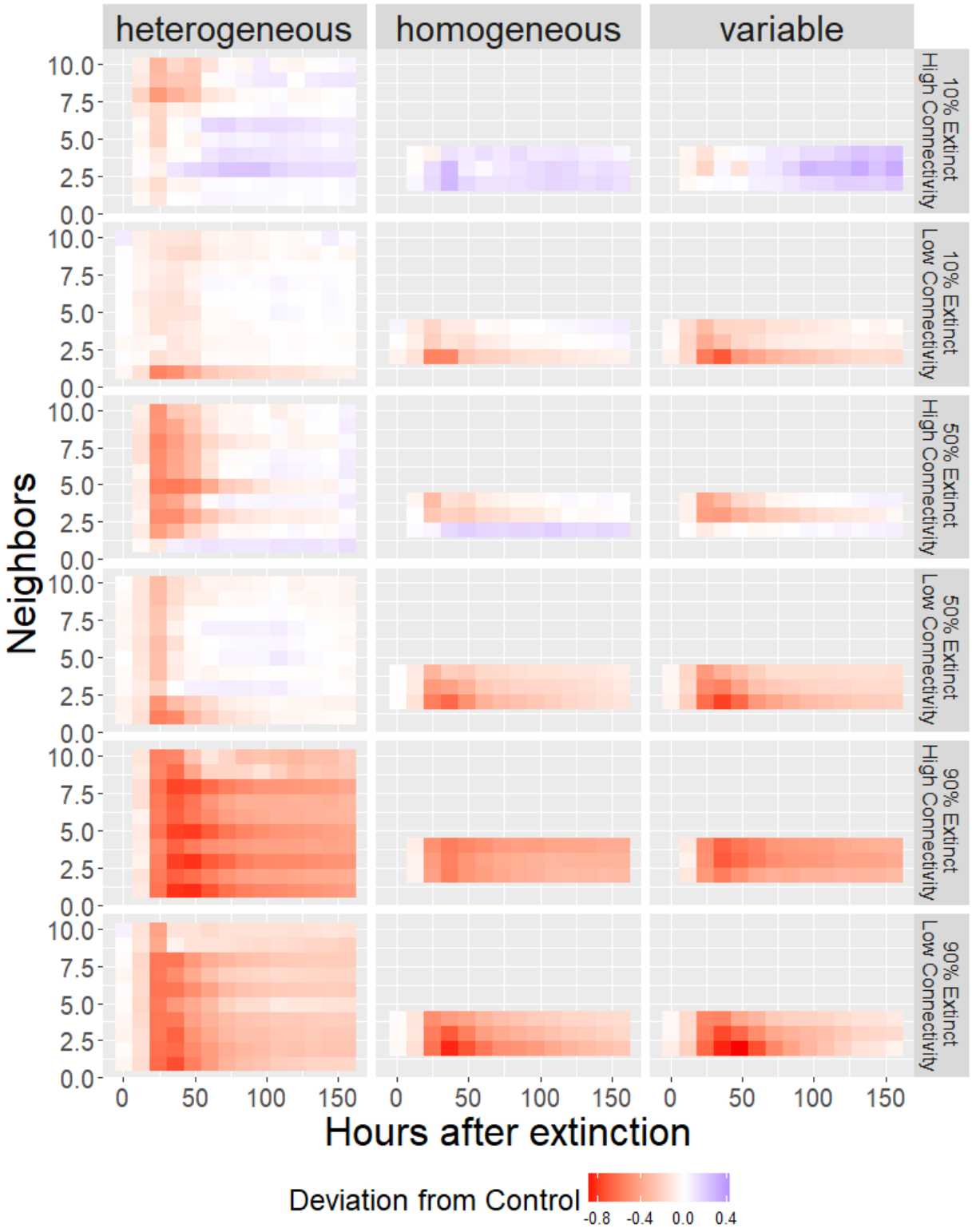

Figure 3.6. Change in deviation from control following extinction across the range of subpopulation connectivities for each combination of corridor arrangement, extinction level, and extinction connectivity for all subpopulations.

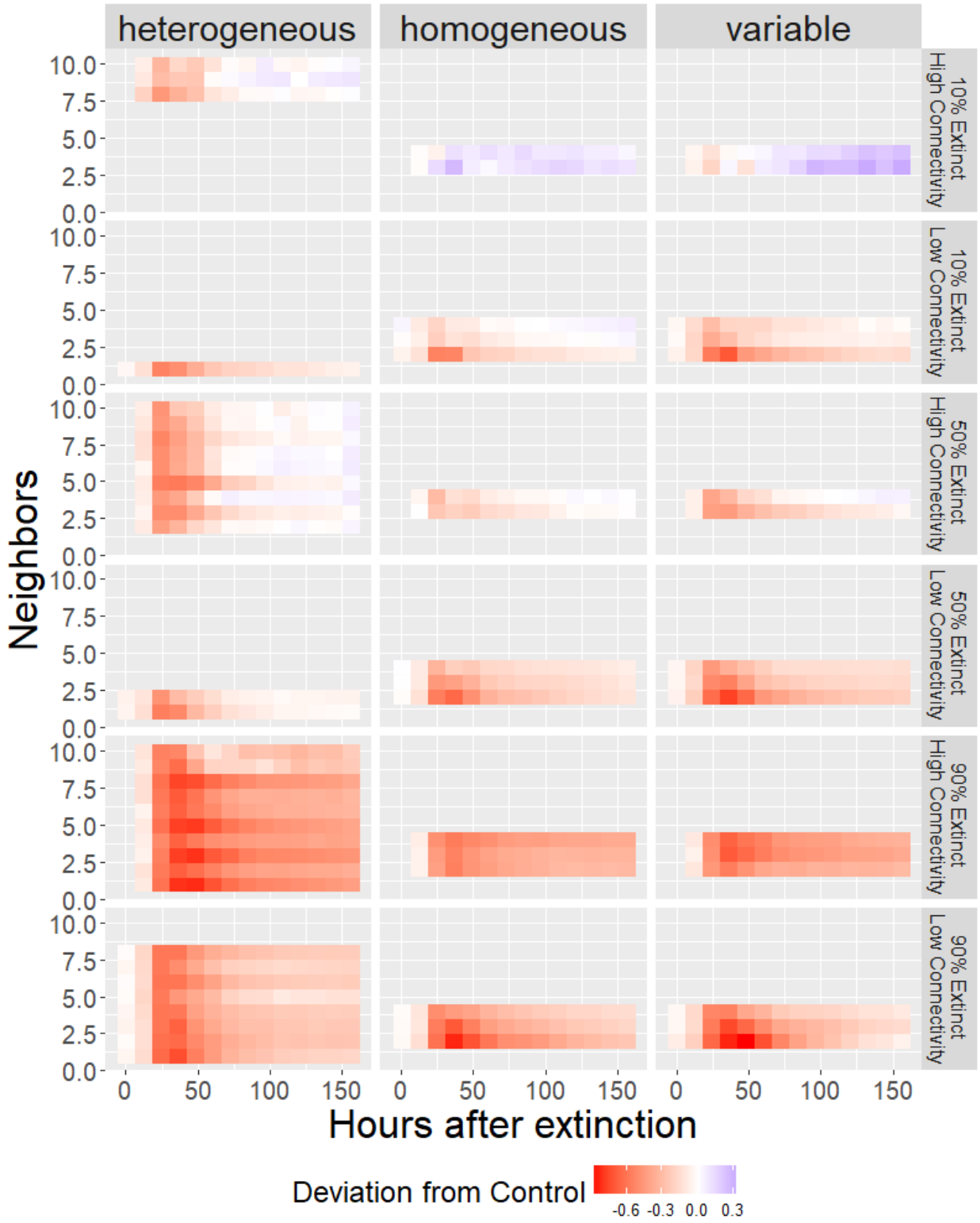

Figure 3.7. Change in deviation from control following extinction across the range of subpopulation connectivities for each combination of corridor arrangement, extinction level, and extinction connectivity for extinct subpopulations only

REFERENCES

Albert, R., Jeong, H., & Barabási, A.-L. (2000). Error and attack tolerance of complex networks. *Nature*, *406*, 378.

Altermatt, F., Fronhofer, E. A., Garnier, A., Giometto, A., Hammes, F., Klecka, J., … Petchey, O. L. (2015). Big answers from small worlds: a user's guide for protist microcosms as a model system in ecology and evolution. *Methods in Ecology and Evolution*, *6*(2), 218–231. doi:10.1111/2041-210X.12312

Amarasekare, P. (1998). Allee Effects in Metapopulation Dynamics. *The American Naturalist*, *152*(2), 298–302. doi:10.1086/286169

Artzy-Randrup, Y., & Stone, L. (2010). Connectivity, Cycles, and Persistence Thresholds in Metapopulation Networks. *PLOS Computational Biology*, *6*(8). doi:10.1371/journal.pcbi.1000876

Beyers, R. J., & Odum, H. T. (1993). *Ecological Microcosms. [electronic resource]*. New York, NY : Springer New York, 1993. Retrieved from https://libproxy.berkeley.edu/login?qurl=http%3a%2f%2fsearch.ebscohost.com%2flogin.aspx%3fdirect%3dtrue%26db%3dcat04202a%26AN%3ducb.b21020315%26site%3deds-live

Boitani, L., Falcucci, A., Maiorano, L., & Rondinini, C. (2007). Ecological Networks as Conceptual Frameworks or Operational Tools in Conservation. *Conservation Biology*, *21*(6), 1414–1422. doi:10.1111/j.1523-1739.2007.00828.x

Brown, J. H., & Kodric-Brown, A. (1977). Turnover Rates in Insular Biogeography: Effect of Immigration on Extinction. *Ecology*, *58*(2), 445–449. doi:10.2307/1935620

Cadotte, M. W. (2007). Competition-Colonization Trade-offs and Disturbance Effects at Multiple Scales. *Ecology*, *88*(4), 823–829. doi:10.1890/06-1117

Carpenter, S. R. (1996). Microcosm Experiments have Limited Relevance for Community and Ecosystem Ecology. *Ecology*, *77*(3), 677–680. doi:10.2307/2265490

Chetkiewicz, C.-L. B., St. Clair, C. C., & Boyce, M. S. (2006). Corridors for Conservation: Integrating Pattern and Process. *Annual Review of Ecology, Evolution, and Systematics*, *37*(1), 317–342. doi:10.1146/annurev.ecolsys.37.091305.110050

Chiu, D. T., deMello, A. J., Di Carlo, D., Doyle, P. S., Hansen, C., Maceiczyk, R. M., & Wootton, R. C. R. (2017). Small but Perfectly Formed? Successes, Challenges, and Opportunities for Microfluidics in the Chemical and Biological Sciences. *Chem*, *2*(2), 201–223. doi:10.1016/j.chempr.2017.01.009

Cold Spring Harbor Protocols. (2006). LB (Luria-Bertani) liquid medium. *Cold Spring Harbor Protocols*, *2006*(1). doi:10.1101/pdb.rec8141

Cowley, D. J., Johnson, O., & Pocock, M. J. O. (2015). Using electric network theory to model the spread of oak processionary moth, Thaumetopoea processionea, in urban woodland patches. *Landscape Ecology*, *30*(5), 905–918. doi:10.1007/s10980-015-0168-6

Dale, M. R. T., & Fortin, M.-J. (2010). From Graphs to Spatial Graphs. *Annual Review of Ecology, Evolution, and Systematics*, *41*(1), 21–38. doi:10.1146/annurev-ecolsys-102209-144718

Dallinger, W. H. (1887). The President's Address. *Journal of the Royal Microscopical Society*, *7*(2), 185–199. doi:10.1111/j.1365-2818.1887.tb01566.x

Dulla, G., & Lindow, S. (2008). Quorum size of Pseudomonas syringae is small and dictated by water availability on the leaf surface. *Proceedings of the National Academy of Sciences*, *105*(8), 3082–3087.

Eriksson, A., Elías-Wolff, F., Mehlig, B., & Manica, A. (2014). The emergence of the rescue effect from explicit within- and between-patch dynamics in a metapopulation. *Proceedings of the Royal Society B: Biological Sciences*, *281*(1780). doi:10.1098/rspb.2013.3127

Estrada, E. (2010). Quantifying network heterogeneity. *Physical Review E*, *82*(6). Retrieved from https://link.aps.org/doi/10.1103/PhysRevE.82.066102

Fagan, W. F. (2002). Connectivity, Fragmentation, and Extinction Risk in Dendritic Metapopulations. *Ecology*, *83*(12), 3243–3249. doi:10.1890/0012-9658(2002)083[3243:CFAERI]2.0.CO;2

Fellous, S., Duncan, A., Coulon, A., & Kaltz, O. (2012). Quorum Sensing and Density-Dependent Dispersal in an Aquatic Model System. *PLOS ONE*, *7*(11), e48436. doi:10.1371/journal.pone.0048436

Fjerdingstad, E. J., Schtickzelle, N., Manhes, P., Gutierrez, A., & Clobert, J. (2007). Evolution of dispersal and life history strategies – Tetrahymena ciliates. *BMC Evolutionary Biology*, *7*(1), 133. doi:10.1186/1471-2148-7-133

Fortuna, M. A., Gómez-Rodríguez, C., & Bascompte, J. (2006). Spatial network structure and amphibian persistence in stochastic environments. *Proceedings of the Royal Society B: Biological Sciences*, *273*(1592), 1429. doi:10.1098/rspb.2005.3448

Fox, J. W., Vasseur, D., Cotroneo, M., Guan, L., & Simon, F. (2017). Population extinctions can increase metapopulation persistence. *Nature Ecology & Evolution*, *1*(9), 1271–1278. doi:10.1038/s41559-017-0271-y

Fraser, L. H., & Keddy, P. (1997). The role of experimental microcosms in ecological research. *Trends in Ecology & Evolution*, *12*(12), 478–481. doi:10.1016/S0169-5347(97)01220-2

Gause, G. F. 1910-1986. (1934). *The struggle for existence, by G. F. Gause*. Baltimore. Retrieved from https://libproxy.berkeley.edu/login?qurl=http%3a%2f%2fsearch.ebscohost.com%2flogin.aspx%3fdirect%3dtrue%26db%3dedsbhl%26AN%3dedsbhl.title.4489%26site%3deds-live

Gilarranz, L. J., & Bascompte, J. (2012). Spatial network structure and metapopulation persistence. *Journal of Theoretical Biology*, *297*, 11–16. doi:10.1016/j.jtbi.2011.11.027

Gilarranz, L. J., Rayfield, B., Liñán-Cembrano, G., Bascompte, J., & Gonzalez, A. (2017). Effects of network modularity on the spread of perturbation impact in experimental metapopulations. *Science*, *357*(6347), 199. doi:10.1126/science.aal4122

Guelzow, N., Muijsers, F., Ptacnik, R., & Hillebrand, H. (2017). Functional and structural stability are linked in phytoplankton metacommunities of different connectivity. *Ecography*, *40*(6), 719–732. doi:10.1111/ecog.02458

Hairston, N. G., Allan, J. D., Colwell, R. K., Futuyma, D. J., Howell, J., Lubin, M. D., … Vandermeer, J. H. (1968). The Relationship between Species Diversity and Stability: An Experimental Approach with Protozoa and Bacteria. *Ecology*, *49*(6), 1091–1101. doi:10.2307/1934492

Hanski, I. (1991). Single-species metapopulation dynamics: concepts, models and observations. *Biological Journal of the Linnean Society*, *42*(1–2), 17–38. doi:10.1111/j.1095-8312.1991.tb00549.x

Hanski, I. (2011). Habitat Loss, the Dynamics of Biodiversity, and a Perspective on Conservation. *Ambio*, *40*(3), 248–255. doi:10.1007/s13280-011-0147-3

Hanski, I., & Ovaskainen, O. (2000). The metapopulation capacity of a fragmented landscape. *Nature*, *404*, 755.

Hawley, J. E., Rego, P. W., Wydeven, A. P., Schwartz, M. K., Viner, T. C., Kays, R., … Jenks, J. A. (2016). Long-distance dispersal of a subadult male cougar from South Dakota to Connecticut documented with DNA evidence. *Journal of Mammalogy*, *97*(5), 1435–1440. doi:10.1093/jmammal/gyw088

Hol, F. J. H., & Dekker, C. (2014). Zooming in to see the bigger picture: Microfluidic and nanofabrication tools to study bacteria. *Science*, *346*(6208). doi:10.1126/science.1251821

Holyoak, M., & Lawler, S. P. (2005). The Contribution of Laboratory Experiments on Protists to Understanding Population and Metapopulation Dynamics. In *Advances in Ecological Research* (Vol. 37, pp. 245–271). Academic Press. doi:10.1016/S0065-2504(04)37008-X

Hothorn, T., Bretz, F., & Westfall, P. (2008). Simultaneous Inference in General Parametric Models. *Biometrical Journal*, *50*(3), 346–363.

Huffaker, C. B. (1958). Experimental studies on predation: Dispersion factors and predator-prey oscillations. *Hilgardia*, *27*(14), 343–383. doi:10.3733/hilg.v27n14p343

Ives, A. R., Foufopoulos, J., Klopfer, E. D., Klug, J. L., & Palmer, T. M. (1996). Bottle or Big-Scale Studies: How do we do Ecology? *Ecology*, *77*(3), 681–685. doi:10.2307/2265491

Jessup, C. M., Forde, S. E., & Bohannan, B. J. M. (2005). Microbial Experimental Systems in Ecology. In *Advances in Ecological Research* (Vol. 37, pp. 273–307). Academic Press. doi:10.1016/S0065-2504(04)37009-1

Jessup, C. M., Kassen, R., Forde, S. E., Kerr, B., Buckling, A., Rainey, P. B., & Bohannan, B. J. M. (2004). Big questions, small worlds: microbial model systems in ecology. *Trends in Ecology & Evolution*, *19*(4), 189–197. doi:10.1016/j.tree.2004.01.008

Kareiva, P. (1989). Renewing the dialogue between theory and experiments in population ecology. In *Perspectives in Ecological Theory* (pp. 68–88). Princeton University Press.

Keitt, T. H. (2003). Network Theory: An Evolving Approach to Landscape Conservation. In V. H. Dale (Ed.), *Ecological Modeling for Resource Management* (pp. 125–134). New York, NY: Springer New York. doi:10.1007/0-387-21563-8_7

Keitt, T., Urban, D., & Milne, B. (1997). Detecting Critical Scales in Fragmented Landscapes. *Conservation Ecology*, *1*(1). Retrieved from https://www.ecologyandsociety.org/vol1/iss1/art4/

Keymer, J. E., Galajda, P., Muldoon, C., Park, S., & Austin, R. H. (2006). Bacterial metapopulations in nanofabricated landscapes. *Proceedings of the National Academy of Sciences*, *103*(46), 17290–17295. doi:10.1073/pnas.0607971103

Levins, R. (1969). Some Demographic and Genetic Consequences of Environmental Heterogeneity for Biological Control. *Bulletin of the Entomological Society of America*, *15*(3), 237–240.

Lou, N., & Peek, K. (2016, February 23). By The Numbers: The Rise Of The Makerspace. *Popular Science*.

McGarigal, K., & Cushman, S. A. (2002). Comparative Evaluation of Experimental Approaches to the Study of Habitat Fragmentation Effects. *Ecological Applications*, *12*(2), 335–345. doi:10.2307/3060945

Millenium Ecosystem Assessment. (2005). *Ecosystems and Human Well-being: Biodiversity Synthesis*. Washington, D.C.: World Resources Institute.

Molofsky, J., & Ferdy, J.-B. (2005). Extinction dynamics in experimental metapopulations. *Proceedings of the National Academy of Sciences of the United States of America*, *102*(10), 3726. doi:10.1073/pnas.0404576102

Monahan, J., Gewirth, A. A., & Nuzzo, R. G. (2001). A Method for Filling Complex Polymeric Microfluidic Devices and Arrays. *Analytical Chemistry*, *73*(13), 3193–3197. doi:10.1021/ac001426z

Morrison, S. A., & Boyce, W. M. (2009). Conserving Connectivity: Some Lessons from Mountain Lions in Southern California. *Conservation Biology*, *23*(2), 275–285. doi:10.1111/j.1523-1739.2008.01079.x

Parker, M. A. (1999). Mutualism in Metapopulations of Legumes and Rhizobia. *The American Naturalist*, *153*(S5), S48–S60. doi:10.1086/303211

Pinheiro, J., Bates, D., DebRoy, S., Sarkar, D., & {R Core Team}. (2017). *{nlme}: Linear and Nonlinear Mixed Effects Models*. Retrieved from https://CRAN.R-project.org/package=nlme

R Core Team. (2016). *R: A Language and Environment for Statistical Computing*. Vienna, Austria: R Foundation for Statistical Computing. Retrieved from https://www.R-project.org/

Resetarits, E., Cathey, S., & Leibold, M. (2018). Testing the keystone community concept: effects of landscape, patch removal, and environment on metacommunity structure. *Ecology*, *99*(1), 57–67. doi:10.1002/ecy.2041

Rosenberg, D. K., & Noon, B. R. (1997). Biological corridors: Form, function, and efficacy. *BioScience*, *47*(10), 677.

Rykiel, E. J. (1996). Testing ecological models: the meaning of validation. *Ecological Modelling*, *90*(3), 229–244. doi:10.1016/0304-3800(95)00152-2

Srivastava, D. S., Kolasa, J., Bengtsson, J., Gonzalez, A., Lawler, S. P., Miller, T. E., … Trzcinski, M. K. (2004). Are natural microcosms useful model systems for ecology? *Trends in Ecology & Evolution*, *19*(7), 379–384. doi:10.1016/j.tree.2004.04.010

Urban, D., & Keitt, T. (2001). Landscape Connectivity: A Graph-Theoretic Perspective. *Ecology*, *82*(5), 1205–1218. doi:10.1890/0012-9658(2001)082[1205:LCAGTP]2.0.CO;2

Urban, D., Minor, E., Treml, E., & Schick, R. (2009). Graph models of habitat mosaics. *Ecology Letters*, *12*(3), 260–273. doi:10.1111/j.1461-0248.2008.01271.x

Warren, P. H. (1996). Dispersal and Destruction in a Multiple Habitat System: An Experimental Approach Using Protist Communities. *Oikos*, *77*(2), 317–325. doi:10.2307/3546071

Wickham, H. (2009). *ggplot2: Elegant Graphics for Data Analysis*. Springer-Verlag New York. Retrieved from http://ggplot2.org

Woodruff, L. L. (1911). The effect of excretion products of Paramaecium on its rate of reproduction. *Journal of Experimental Zoology*, *10*(4), 557–581. doi:10.1002/jez.1400100407